BRAIN
ORIGINAL ARTICLE

CCL2 blockade combined with PD-1/P-selectin immunomodulators impedes breast cancer brain metastasis

Sahar Israeli Dangoor,[1] Rami Khoury,[1] Koren Salomon,[1] Sabina Pozzi,[1] Shir Shahar,[1] Adan Miari,[1] Yael Leichtmann-Bardoogo,[2] Neta Bar-Hai,[3,4] Neta Frommer,[1] Eilam Yeini,[1] Tom Winkler,[5] Nora Balint Lahat,[6] Iris Kamer,[3] Ori Hadad,[1] Kathrin Laue,[5] Henry Brem,[7] Thomas M. Hyde,[8,9,10] Jair Bar,[3] Iris Barshack,[6,11] Uri Ben-David,[5] Dana Ishay-Ronen,[3,4] Ben M. Maoz[2,12,13,14] and Ronit Satchi-Fainaro[1,12,14]

Over the last two decades, the diagnosis and treatment of breast cancer patients have improved considerably. However, brain metastases remain a major clinical challenge and a leading cause of mortality. Thus, a better understanding of the pathways involved in the metastatic cascade is essential.

To this end, we have investigated the reciprocal effects of astrocytes and breast cancer cells, employing traditional 2D cell culture and our unique 3D multicellular tumouroid models.

Our findings revealed that astrocytes enhance the proliferation, migration and invasion of breast cancer cells, suggesting a supportive role for astrocytes in breast cancer outgrowth to the brain. Elucidating the key players in astrocyte-breast cancer cells crosstalk, we found that CCL2 is highly expressed in breast cancer brain metastases tissue sections from both patients and mice. Our *in vitro* and *in vivo* models further confirmed that CCL2 has a functional role in brain metastasis. Given their aggressive nature, we sought additional immune checkpoints for rationale combination therapy. Among the promising candidates were the adhesion molecule P-selectin, which we have recently shown to play a key role in the crosstalk with microglia cells and the co-inhibitory receptor PD-1, the main target of currently approved immunotherapies. Finally, combining CCL2 inhibition with immunomodulators targeting either PD-1/PD-L1 or P-selectin/P-Selectin Ligand-1 axes in our human 3D tumouroid models and *in vivo* presented more favourable outcomes than each monotherapy.

Taken together, we propose that CCL2-CCR2/CCR4 is a key pathway promoting breast cancer brain metastases and a promising target for an immunotherapeutic combination approach.

1 Department of Physiology and Pharmacology, Faculty of Medicine, Tel Aviv University, Tel Aviv 6997801, Israel
2 Department of Biomedical Engineering, Tel Aviv University, Tel Aviv 6997801, Israel
3 Cancer Research Center, Oncology Institute, Sheba Medical Center, Tel-Hashomer 5262000, Israel
4 Affiliated with Faculty of Medicine, Tel Aviv University, Tel Aviv 6997801, Israel
5 Department of Human Molecular Genetics and Biochemistry, Faculty of Medicine, Tel Aviv University, Tel Aviv 6997801, Israel
6 Department of Pathology, Sheba Medical Center, Tel Hashomer 5262000, Israel
7 Department of Neurosurgery, Johns Hopkins University School of Medicine, Baltimore, MD 21218, USA
8 Lieber Institute for Brain Development, Johns Hopkins Medical Campus, Baltimore, MD 21218, USA
9 Department of Psychiatry & Behavioral Science, Johns Hopkins University School of Medicine, Baltimore, MD 21218, USA

Received March 30, 2024. Revised September 11, 2024. Accepted October 08, 2024. Advance access publication October 25, 2024

10 Department of Neurology, Johns Hopkins University School of Medicine, Baltimore, MD 21218, USA
11 Department of Pathology, Faculty of Medicine, Tel Aviv University, Tel Aviv 6997801, Israel
12 Sagol School of Neuroscience, Tel Aviv University, Tel Aviv 6997801, Israel
13 Sagol Center for Regenerative Medicine, Tel Aviv University, Tel Aviv 6997801, Israel
14 The Center for Nanoscience and Nanotechnology, Tel Aviv University, Tel Aviv 6997801, Israel

Correspondence to: Prof. Ronit Satchi-Fainaro, PhD
Department of Physiology and Pharmacology
Faculty of Medicine, Tel Aviv University
Tel Aviv 6997801, Israel
E-mail: ronitsf@tauex.tau.ac.il

Keywords: breast cancer brain metastasis; 3D cancer models; astrocytes; CCL2; P-selectin; PD-1

Introduction

Breast cancer is the most common malignancy in women and the leading cause of cancer-related deaths in women worldwide.[1] For locally invasive breast cancer, the 5-year survival rate is above 99%. This rate dramatically decreases to 30% when the disease is spread to distant metastatic sites.[2] Breast cancer is one of the main cancer types metastasizing to the brain, with approximately 15% of patients developing CNS metastases, presenting an even higher incidence in autopsies. The survival rate declines even further if the metastatic disease involves the CNS, with a 1-year survival rate of only 20%,[3-5] while suffering from reduced quality of life.[4]

In the last two decades, the diagnosis and treatment of breast cancer, including patients at the metastatic stage, have improved considerably. However, the incidence of breast cancer brain metastasis (BCBM) is increasing due to earlier detection and longer survival from the primary tumour. Hence, it is still a major clinical problem and leading cause of death from cancer.[3,4,6,7]

The treatment options for BCBM include stereotactic radiosurgery (SRS), chemotherapy, targeted therapy according to the primary tumour subtype, surgical resection and whole-brain radiation therapy (WBRT).[8] Unfortunately, the therapeutic benefits of current treatment options are limited.[4] Thus, it is crucial to gain a better understanding of the pathways that orchestrate the metastatic cascade in BCBM.

In extracranial malignancies, it is well established that the tumour microenvironment has an essential role in cancer progression and organ-specific metastasis.[5,9,10] In recent years, it has become clear that the unique brain tumour microenvironment (bTME) also plays a role in the pathology of primary and metastatic brain tumours.[11-14] Data gathering with regard to specific therapeutic targets in BCBM has begun in recent years,[15-17] and the involvement of the bTME in BCBM development and progression is becoming evident.[18-21]

Brain tumours in both animal models and patients usually encompass reactive astrocytes.[22-25] Astrocytes are responsible for brain homeostasis and do not proliferate in normal adult brains. However, in response to brain injury, astrocytes can be activated, leading to astrogliosis and glial scar formation. Similarly, brain metastases (BM) induce the local activation of astrocytes, neuroinflammation and astrogliosis.[12,26] Furthermore, astrocytes can support the formation and progression of BM by communicating with the cancer cells via secreted factors (e.g. cytokines, enzymes and neurotrophic factors), and the inhibition of such factors can lead to the prevention or regression of BM depending on the disease stage.[14,27,28]

Activated microglia are also often found near and within brain tumours.[23,29-32] Microglia are macrophage-like cells and serve as brain-resident immune cells. They play diverse roles in cancer, which could be attributed to their heterogeneity and different activation states.[27] Microglial cells can lead to cancer-promoting effects by secreting factors such as cytokines, growth factors and enzymes,[11,23,31,33,34] and glioma proliferation can be attenuated by the inhibition of microglial activation.[29] On the other hand, it has also been reported that microglia can elicit cytotoxicity against BM from lung cancer.[35]

These findings demonstrate that upon arrival in the brain, extensive direct and indirect crosstalk between brain resident cells and tumour cells occurs, resulting in a multitude of pathway activations both in tumour and host cells. Furthermore, the tumour cells that succeed in colonizing the brain appear to have gained the ability to exploit brain endogenous substrates that are naturally secreted by the resident cells as oncogenic signals.[6] Understanding the contribution of interactions between metastatic breast cancer cells and host bTME cells to brain metastasis colonization may provide a novel therapeutic approach to prevent BM formation.

Here, we show that via secretion of CCL2, astrocytes support BCBM by enhancing the tumourigenic properties of breast cancer cells, such as proliferation, migration and invasion. CCL2 (also known as monocyte chemoattractant protein-1; MCP-1) is a low molecular weight cytokine with chemoattractant activity (i.e. chemokine),[36] and CCR2 and CCR4 are the receptors that are known to bind it.[37] Additional promising targets for combination therapy are the adhesion molecule P-selectin (SELP) and its ligand (PSGL-1), as well as the co-inhibitory receptor programmed cell death protein-1 (PD-1) and its ligand (PD-L1). We have recently shown that the SELP-PSGL-1 axis is involved in glioblastoma-microglia crosstalk and is a key regulator of glioblastoma progression.[11] Additionally, immunotherapies are becoming reasonable treatment options, as the involvement of the immune system in breast cancer progression has recently been re-evaluated.[38] In melanoma and non-small cell lung cancer (NSCLC) BM, targeting PD-1 or PD-L1 has already shown intracranial efficacy.[39,40] Collectively, our findings outline the CCL2-CCR2/CCR4 axis as a key player in astrocyte-breast cancer cell crosstalk during the BCBM cascade and offer a potential new combined immunotherapeutic approach to treating this devastating disease.

Materials and methods

Breast cancer 3D tumour spheroids

Multicellular tumour spheroids were prepared using a modification of the hanging-drop method,[41] in which droplets of cell suspension are

held hanging from the bottom of an inverted tissue-culture plate until cells agglomerate spontaneously at the lower part of the droplet due to gravity. Full details can be found in the Supplementary material.

BBB co-culture and BBB-chip with astrocytes and MDA-MB-231 cells

Experiments were performed using two platforms: (i) a commercial 24-well Transwell® (Costar Corp., Corning); and (ii) a blood–brain barrier (BBB)-chip platform (Supplementary Fig. 16A) that was fabricated as previously described.[42,43] For both platforms, brain microvascular endothelial cells (BMEC) were seeded as mentioned in the Supplementary material. The following day, the underpart of the membrane was coated with 3% Matrigel for 1 h, then human primary astrocytes (ScienCell, 1800-scl) were seeded at a ratio of 1:2 astrocytes:BMEC. Astrocytes were incubated for at least 1 h before flipping the membrane into the BMEC well containing endothelial serum-free medium supplemented with B27, 100 U/ml penicillin and 100 µg/ml streptomycin. Human primary brain vascular pericytes (ScienCell 1200-scl) were seeded on top of the BMEC layer at a ratio of 1:3 pericytes:BMEC. Barrier function was evaluated by trans-epithelial electrical resistance (TEER) measurements (Millicell ERS-2 Volt-Ohm Meter, Merck Millipore) daily.

mCherry-labelled MDA-MB-231 cells (1×10^5) were added to the upper side of the Transwell and treated with 0.3 mM bindarit, 1 µg/ml CCL2 or not treated (control). TEER values were followed for up to 24 h after MDA-MB-231 cell administration. Cells on Transwells were then fixed with 4% paraformaldehyde (PFA) for 10 min following Dulbecco's phosphate buffered saline (PBS) washes and immunostaining.

Gene expression analysis

Gene expression data were downloaded from the Gene Expression Omnibus database https://www.ncbi.nlm.nih.gov/geo/ (accession number GSE12276). mRNA expression levels of CCL2 (216598_s_at), CCR2 (206978_at), CCR4 (208376_at), SELP (206049_at), SELPLG (209879_at), CD274 (223834_at) and PDCD1 (207634_at) were compared between primary tumours that relapsed to the brain and breast tumours that relapsed to other distant organs, using a one-tailed non-paired Student's *t*-test.

Tumour spheroids for drug combination

To assess the effect of immunotherapeutic drug combinations, multicellular tumour spheroids were prepared using the liquid overlay technique,[44] in which the cell suspension is seeded in round-bottom ultra-low attachment microplates, and the cells agglomerate spontaneously at the lower part of the well due to gravity. The full details can be found in the Supplementary material.

Breast cancer 4T1 intracranial animal model

To generate primary breast cancer prior to BCBM, 4T1 cells (3×10^5 cells/100 µl) were inoculated into the mammary fat pad of immunocompetent 8-week-old female BALB/c mice (Envigo, CRS). Tumour growth was measured using callipers, and the tumour volume was calculated using the standard formula: length × width^2 × 0.52. Once they reached a volume of 70 mm^3, the primary lesions were resected. For drug efficacy studies, 4T1 cells (2×10^4 cells/2 µl) were stereotactically inoculated into the striatum (2 mm left from the bregma and 3.5 mm depth) of the same mice (previously bearing the primary tumour). Three days following cell inoculation, mice were treated intravenously (i.v.) with 100 mg/kg bindarit or the corresponding vehicle every other day (QOD) i.v. with 16 mg/kg SELPi or the corresponding vehicle QOD and intraperitoneally (i.p.) with 10 mg/kg Anti-Mouse PD-1 *in vivo* antibody or PBS twice a week. Fourteen days post intracranial breast cancer cell inoculation, four mice per group were euthanized, blood was collected, and mice were immediately perfused with 4% PFA in PBS. Brains were then harvested for further immunostaining analysis. Mouse body weight was monitored three times a week, and tumour growth was followed twice a week using 4.7 T/1 H MRI. Mice were euthanized when they lost 10% body weight in a week, had lost 20% of their initial weight or when neurological symptoms appeared.

Randomization and assignment of mice to the treatment groups

To avoid bias in the results, before starting the treatments, all mice were randomly assigned to one of the treatment groups.

Human specimens

Formalin-fixed paraffin-embedded (FFPE) breast cancer samples (BM, $n = 36$; primary breast cancer, $n = 18$; adjacent breast tissue, $n = 5$), FFPE lung cancer samples (BM, $n = 26$; primary lung cancer, $n = 17$; normal lung tissue, $n = 6$) and frozen peripheral blood mononuclear cells (PBMCs) from healthy donors ($n = 10$) were obtained from Sheba Medical Center following the receipt of informed consent. The manipulation of the human samples for immunostaining was accepted by the ethics committees of Tel Aviv University and Sheba Medical Center, under an approved Institutional Review Board (IRB) protocol (5727-18-SMC). Healthy human brain samples were collected by Thomas Hyde at the Lieber Institute for Brain Development as described under an approved IRB protocol (90-M-0142).

Statistical analyses

Data are expressed as mean ± standard deviation (SD) for *in vitro* assays or ± standard error of the mean (SEM) for *in vivo* and *ex vivo* assays. Unless otherwise stated, statistical significance was determined using an unpaired, two-sided *t*-test when comparing two groups and multiple comparisons ANOVA test when comparing more than two groups. $P < 0.05$ was considered statistically significant. For Kaplan–Meier survival curves, *P*-values were determined using a log-rank survival analysis test, with further adjustment of *P*-values using Holm–Šídák analysis. Statistical analysis was performed using GraphPad Prism 10 (GraphPad Software, Boston, MA).

No statistical method was used to predetermine the sample size. The sample size was chosen to be adequate to receive significant results as determined by preliminary experiments and based on previous publications of multiple groups in the field.[18,45-47]

Results

Astrocyte–breast cancer cell crosstalk enhances proliferation, migration and invasion

To evaluate the role of astrocytes in BCBM progression, we utilized both traditional 2D co-culture and 3D multicellular cancer models. In line with previous reports on the tumourigenic effect of astrocytes on MDA-MB-231 breast cancer cells,[48] our investigations revealed that both murine and human mammary adenocarcinomas, 4T1 and MDA-MB-231 cells, respectively, present increased proliferation rates when co-cultured with primary astrocytes, in a dose-

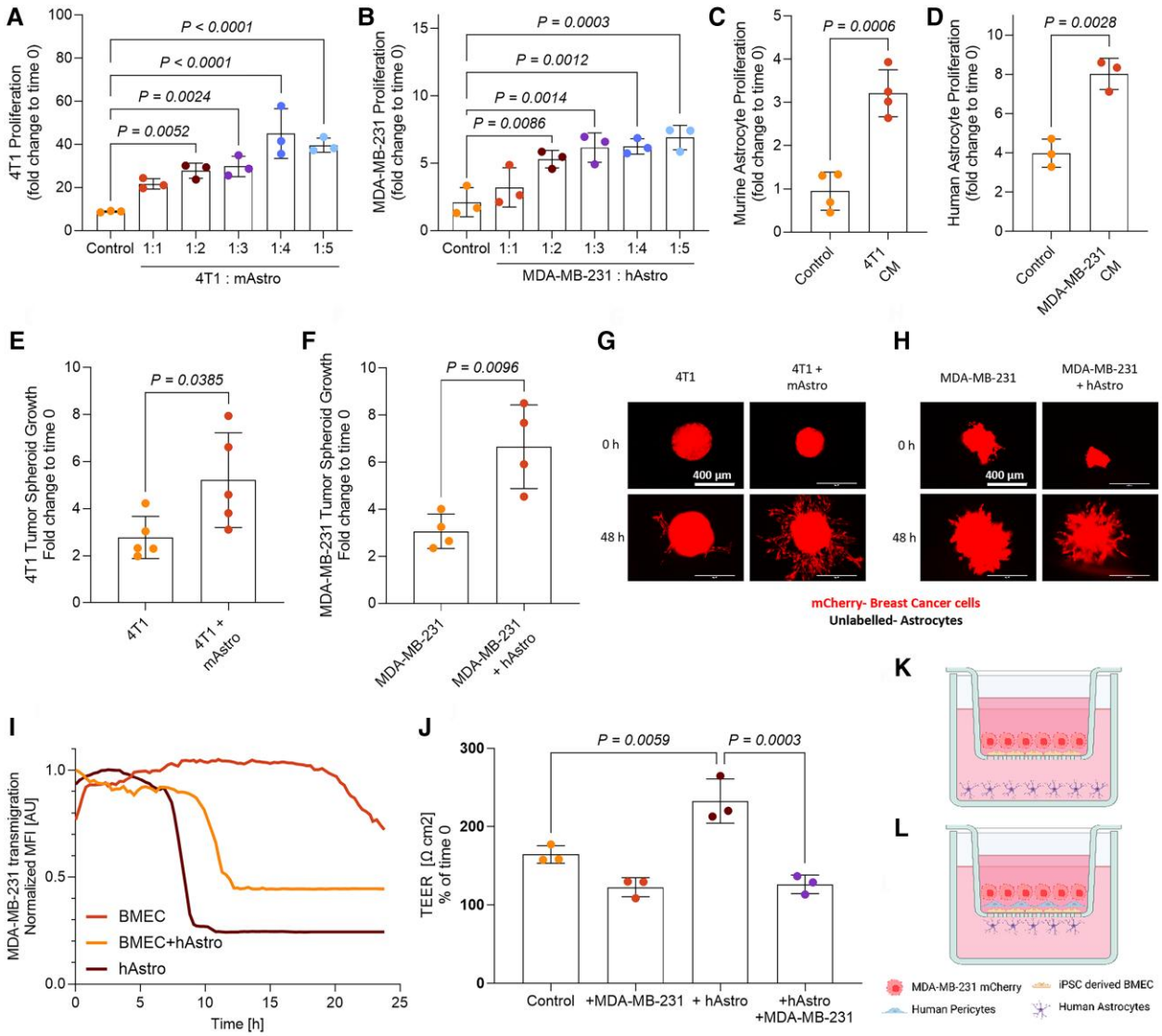

Figure 1 Astrocytes and breast cancer cells engage in reciprocal interactions. (**A** and **B**) Proliferation rates after 96 h of (**A**) iRFP-labelled murine 4T1 cells in the presence or absence of murine astrocytes ($n = 3$) and (**B**) iRFP-labelled human MDA-MB-231 cells in the presence or absence of human astrocytes ($n = 3$). Data are represented as fold-change to time 0. Statistical significance was determined using one-way ANOVA and Dunnett's multiple comparisons test. (**C** and **D**) Proliferation rates after 190 h of (**C**) murine astrocytes in the presence or absence of 4T1 conditioned medium ($n = 4$) and (**D**) human astrocytes in the presence or absence of MDA-MB-231 conditioned medium ($n = 3$). Data are represented as fold-change to time 0. (**E** and **F**) Quantification of tumour spheroids area after 48 h of (**E**) mCherry-labelled 4T1 cells in the presence or absence of murine astrocytes ($n = 5$) and (**F**) mCherry-labelled MDA-MB-231 cells in the presaence or absence of human astrocytes ($n = 4$). Data are presented as fold-change to time 0. (**G** and **H**) Representative images of tumour spheroids from **E** and **F**, respectively. Scale bar = 400 µm. (**I**) Quantification of mCherry-labelled MDA-MB-231 trans-endothelial cells and/or trans-astrocytic migration, presented by the MDA-MB-231 mCherry signal recorded on the surface level of the Transwell® membrane. Reduction in the fluorescent signal indicates the transmigration of the cells through the barrier ($n = 1$). (**J**) Trans-epithelial electrical resistance (TEER) values of a barrier consisting of induced pluripotent stem cell (iPSC)-derived brain microvascular endothelial cells (BMEC) and human pericytes, with or without human astrocytes and mCherry-labelled MDA-MB-231 measured 20 h after the addition of MDA-MB-231 cells. Data represented as % of time 0. Statistical significance was determined using one-way ANOVA and Tukey's multiple comparisons test. (**K–L**) Illustration of the blood–brain barrier (BBB) models used in **I** and **J**, respectively. This image was created with BioRender.com. All data are expressed as mean ± standard error; Unless otherwise stated, statistical significance was determined using an unpaired Student's *t*-test. CM = conditioned medium; hAstro = human astrocytes; mAstro = murine astrocytes.

dependent manner (Fig. 1A and B). The relevance of the selected cell ratios was confirmed in an *in vivo* EMT6 mouse model by analysis of GFAP-positive astrocytes in the vicinity of the tumour region. Staining and analysing cell ratios revealed 1.657 more astrocytes than cancer cells in the tumour area (Supplementary Fig. 1), suggesting that the range of ratios of 1:1 and 1:2 that we selected are physiologically relevant. The higher cell ratios (1:3, 1:4, 1:5) clearly show the dose-dependent effect that astrocytes have on breast cancer proliferation.

In addition, the presence of 4T1 conditioned medium (CM) or MDA-MB-231 CM, which contains cancer cell-secreted factors, increased the proliferation rates of murine and human astrocytes, respectively (Fig. 1C and D). Using a Transwell migration assay, we found a significant increase in 4T1 cell migration towards murine

primary astrocytes (mAstro) and MDA-MB-231 cell migration towards human primary astrocyte (hAstro) CM (Supplementary Fig. 2A and B). The same effect was found with another murine breast cancer cell line, EMT6, which is BRCA-mutated (Supplementary Fig. 2C).

We further characterized the mutual interactions between breast cancer cells and the brain metastatic niche in a 3D model to better mimic the bTME. To that end, we established a 3D multicellular BCBM spheroid model containing breast cancer cells, astrocytes and brain endothelial cells, separately or combined. These spheroids were created using a modified hanging drop method[41] and later transferred into basement membrane extracts. Utilizing this model, we assessed the proliferation, migration and invasion of the breast cancer cells by monitoring the 3D spheroids using live imaging (based on the fluorescence signal of the breast cancer cells).

Supporting the results obtained from the classic 2D culture assays, we identified a significant increase in the growth and sprouting of breast cancer cells in 3D BCBM spheroids containing astrocytes compared with spheroids containing breast cancer cells only (Fig. 1E–H). In addition, the presence of the BBB human cerebral microvascular endothelial cells (hCMEC/D3) increased MDA-MB-231 3D spheroid growth and sprouting (Supplementary Fig. 2D and E).

As an additional model of the bTME, we created an advanced BBB model composed of induced pluripotent stem-cell (iPSC)-derived BMEC, primary human pericytes (optional) and hAstro, using both the Transwell and BBB-chip[42,49] platforms. We monitored the TEER values until the impedance was $>1000\,\Omega \times cm^2$, indicating good barrier function, before starting the experiments. Interestingly, the addition of astrocytes increased the TEER values, indicating a tighter barrier, while the addition of MDA-MB-231 cells impaired the barrier, as indicated by lower TEER values (Fig. 1J). As expected, the transmigration of MDA-MB-231 cells through the barrier lacking any cells towards astrocytes was much faster than the transmigration through the BMEC barrier (Fig. 1I and Supplementary videos 1 and 2). Adding astrocytes to the endothelial system significantly increased MDA-MB-231 trans-endothelial migration, which also occurred faster compared with the BMEC-only barrier (Fig. 1I and Supplementary videos 2 and 3). This showed that although astrocytes enhance barrier integrity, their crosstalk with breast cancer cells increases trans-endothelial migration.

CCL2-CCR2/4 axis is upregulated in breast cancer metastasis

Following the elucidation of the reciprocal effects between astrocytes and breast cancer cells, we aimed to identify the secreted factors involved in this intercommunication. Therefore, we performed cytokine arrays on 4T1 cells co-cultured with mAstro and MDA-MB-231 cells co-cultured with hAstro, in which a set of upregulated cytokines was found (Fig. 2A and B and Supplementary Fig. 2A and B). We identified CCL2 as one of the factors secreted at an exceptionally high level in the co-culture conditions, and it was upregulated both in the human and the murine models (Fig. 2A and B and Supplementary Fig. 3A and B).

Taken together, we decided to focus on the role of the CCL2-CCR2/CCR4 axis in breast cancer cell–astrocyte interactions. The expression of these markers was validated on tissue sections from the 4T1 BCBM mouse model. First, we injected 4T1 cells orthotopically into the mammary fat pad of immunocompetent female BALB/c mice and, following surgical removal of the primary tumour, we performed intracranial cell injection in the same mice. Resembling the expression levels found in humans, all three markers, CCL2, CCR2 and CCR4, presented high levels in the mice BM, in comparison with the primary tumours and normal breast and brain tissues (Fig. 2C and E–G). The presence of these three markers was also confirmed in BM of a spontaneous model of intracardially injected EMT6 cells (Supplementary Fig. 6A and B). To verify the clinical relevance of these findings, we validated the expression of CCL2, CCR2 and CCR4 by immunohistochemistry (IHC) staining of FFPE clinical samples of BCBM. We found that CCL2 and CCR2 are highly overexpressed in BM and primary breast cancer, compared with normal breast and brain tissues (Fig. 2D, H and I). Even though CCR4 presented generally lower expression levels than CCR2, it was also overexpressed in the BM samples (Fig. 2D and J). We further analysed the expression levels using data from primary tumours of breast cancer patients that later metastasized to the brain or other organs (GSE12276).[50] Although not reaching statistical significance, all three markers, CCL2, CCR2 and CCR4, showed a trend towards higher expression in the tumours that later metastasized to the brain (Fig. 2K–M).

To further validate the expression of CCL2, we performed ELISA assays measuring the protein secretion level. In agreement with our findings derived from the cytokine arrays, higher secretion of CCL2 was demonstrated when 4T1 or MDA-MB-231 cells were co-cultured with astrocytes, compared with the respective monocultures (Fig. 3A and B).

To reveal the main source of CCL2, we further validated the mRNA expression level of CCL2 using RT-qPCR. 4T1 cells and mAstro were grown in each other's CM, astrocyte starvation medium (0% serum) or full astrocyte medium. mCherry-labelled MDA-MB-231 cells and iRFP-labelled hAstro were mono- or co-cultured and then sorted by their fluorescence. We found that the activation with starvation medium increased CCL2 expression by mAstro, and when cultured in 4T1 CM, mAstro CCL2 expression was further increased (Fig. 3C). When MDA-MB-231 and hAstro were co-cultured, the astrocytes expressed much higher levels of CCL2, compared with the monocultures (Fig. 3D). These findings indicated that astrocytes are the primary source of CCL2 secreted in the astrocyte–breast cancer cell crosstalk.

To validate the activation state of the astrocytes that are the main source of the secreted CCL2, we performed a fluorescence-activated cell sorting (FACS) analysis. We exposed murine astrocytes to either 4T1 serum-free medium (SFM) (negative activation), 4T1 SFM supplemented with lipopolysaccharide (LPS) (positive activation) or 4T1 CM and tested the resulting expression of intracellular CCL2 in two types of astrocytic populations: (i) activated/reactive astrocytes [GLAST negative (–), GFAP positive (+)]; and (ii) non-GFAP activated astrocytes (GLAST+, GFAP–). Our results revealed that non-activated astrocytes (GLAST+, GFAP–) generally express much less CCL2 than the activated astrocytes (GLAST–, GFAP+), and the different activation media influence the level of CCL2 expression by the activated astrocytes (Fig. 3E and F). The exposure of mAstro to breast cancer cell-secreted factors from the 4T1 CM induced the highest CCL2 expression by the activated astrocytes in the culture (Fig. 3E).

In addition, we assessed the expression levels of the receptors for CCL2 by flow cytometry. CCR2 and CCR4 were both expressed on the surface of 4T1 and MDA-MB-231 cells. When activated with a starvation medium, both cell lines presented an increased level of CCR2 and CCR4, with a further increase when cultured in astrocyte CM (Fig. 3G–N).

As melanoma, breast and lung cancer are the leading three primary tumour sites metastasizing to the brain,[5] and we have previously established the importance of CCL2 in the context of melanoma brain metastasis,[14] we searched for evidence that the CCL2 pathway is important for the brain metastatic process in

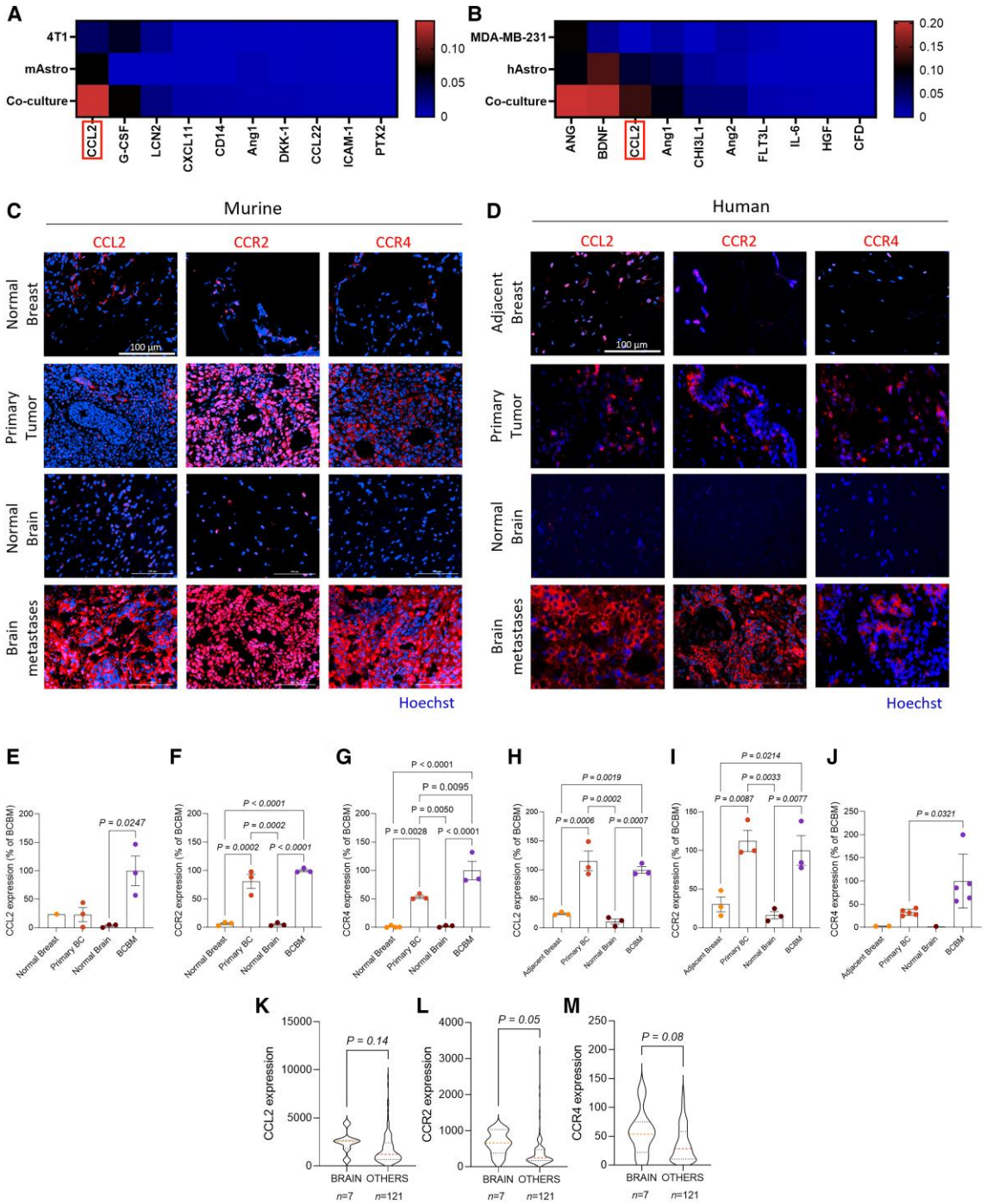

Figure 2 CCL2–CCR2/4 axis is upregulated in human and murine breast cancer brain metastasis models and patient samples. (**A** and **B**) Cytokine arrays of media collected following 72 h of cell culturing from mono-cultures and co-cultures of (**A**) Murine 4T1 cells and murine astrocytes ($n = 1$) and (**B**) Human MDA-MB-231 cells and human astrocytes ($n = 1$). Membrane negative controls were subtracted, and data were normalized to membrane reference spots and expressed per million cells. The 10 most upregulated cytokines are presented for each cell line, determined by the fold-change in the co-culture compared to the average of the mono-cultures. Green indicates low expression, and red indicates high expression. (**C** and **D**) CCL2–CCR2/CCR4 (red), Hoechst (blue) staining of brain metastases, primary breast cancer, adjacent/normal breast and normal brain in (**C**) murine tissue sections and (**D**) human tissue sections. Scale bars = 100 µm. Representative images of selected fields (the highest expressing fields are presented). (**E–G**) Quantification of the immunostained murine tissues from **C**. Data are expressed as mean ± standard error of the mean (SEM). Statistical significance was determined using one-way ANOVA and Tukey's multiple comparisons tests. (**H–J**) Quantification of the immunostained human tissues from **D** (**H** and **I**, $n = 3$ and **J**, $n = 1$–5 fields per sample). Data are expressed as mean ± SEM. Statistical significance was determined using one-way ANOVA and Tukey's multiple comparisons tests for **H** and **I** and unpaired Student's *t*-test for **J**. Dots on the graph in **J** represent technical repeats. (**K–M**) mRNA expression analysis of (**K**) CCL2, (**L**) CCR2 and (**M**) CCR4 on human primary breast tumours that metastasized to the brain, compared with primary tumours that metastasized to other organs. Data are presented as violin plots, showing median and quartiles. Statistical significance was determined using a one-tailed unpaired Student *t*-test. ANG = Angiogenin; Ang1 = Angiopoietin-1; Ang2 = Angiopoietin-2; BC = breast cancer; BCBM = breast cancer brain metastases; CFD = Complement Factor D; CHI3L1 = Chitinase 3-like 1; FLT3L = Flt-3 ligand; hAstro = human astrocytes; LCN2 = Lipocalin-2; mAstro = murine astrocytes; PTX2 = Pentraxin 2.

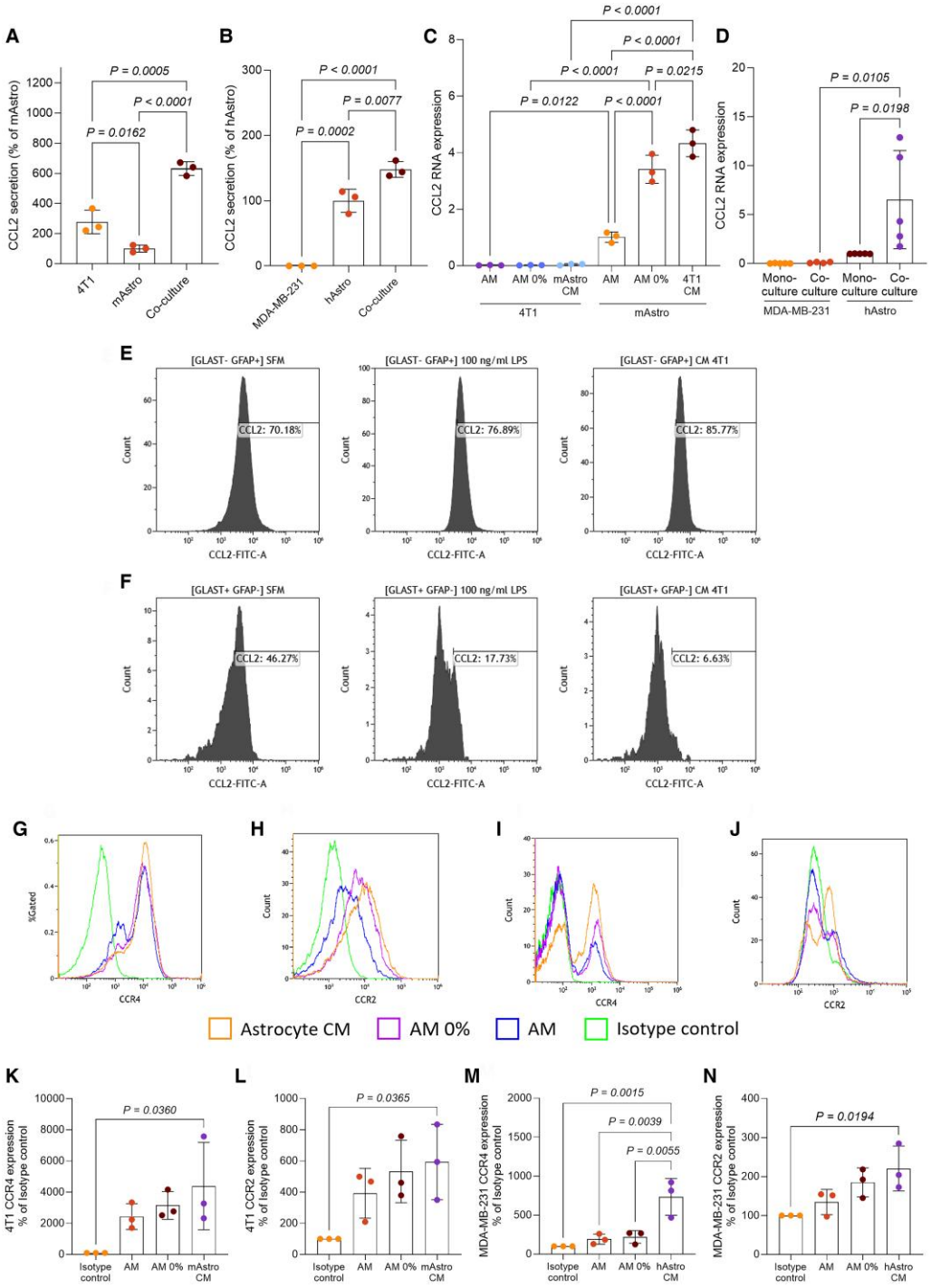

Figure 3 The CCL2–CCR2/CCR4 axis is upregulated in breast cancer brain metastases *in vitro* models. (**A** and **B**) CCL2 secretion measured by ELISA of media collected after 72 h of cell culturing, from mono-cultures and co-cultures of (**A**) Murine 4T1 cells and murine astrocytes ($n = 3$) and (**B**) human MDA-MB-231 cells and human astrocytes ($n = 3$). Data expressed as % of astrocyte secretion. (**C** and **D**) CCL2 mRNA expression measured by reverse transcription qPCR of RNA extracted from cancer cells and astrocytes: (**C**) 4T1 cells cultured in astrocyte medium (AM), astrocyte starvation medium (AM 0%, 0% fetal bovine serum) or murine astrocyte conditioned medium (CM); and murine astrocytes cultured in AM, AM 0% or 4T1 CM (one representative of $n = 3$; dots on the graph represent technical repeats). Data are expressed as fold-change compared to murine astrocytes in AM. (**D**) mCherry-labelled MDA-MB-231 cells and iRFP-labelled human astrocytes after sorting the cells by their fluorescence labels from either mono- or co-cultures ($n = 5$). Data are expressed as fold-change compared with the human astrocytes from monoculture. (**E** and **F**) Fluorescence-activated cell sorting (FACS) analysis of murine astrocytes for the intracellular CCL2 expression following exposure to 4T1 serum-free medium (SFM), 4T1 SFM supplemented with lipopolysaccharide (LPS) or 4T1 CM. The analysis was performed for two types of astrocytic populations: (**E**) Activated/reactive astrocytes [gated for GLAST negative (–), GFAP positive (+)] and (**F**) non-GFAP-activated astrocytes (gated for GLAST+, GFAP–). (**G** and **H**) FACS analysis of 4T1 cells in murine astrocyte medium ($n = 3$) of (**G**) CCR4 expression and (**H**) CCR2 expression. (**I** and **J**) FACS analysis of MDA-MB-231 cells in human astrocyte medium ($n = 3$) of (**I**) CCR4 expression and (**J**) CCR2 expression. (**K**–**N**) Quantification of mean fluorescence intensity of cells from **G**–**J**. All data are expressed as mean ± standard deviation. Unless otherwise stated, statistical significance was determined using one-way ANOVA and Tukey's multiple comparisons tests. hAstro = human astrocytes; mAstro = murine astrocytes.

general and not limited to breast cancer only. Thus, we also investigated this phenomenon in lung cancer brain metastasis.

We characterized lung cancer brain metastases specimens from both clinical samples and our mouse models by IHC. The immunostaining analysis revealed that CCL2, CCR2 and CCR4 are highly expressed in primary lung cancer (Supplementary Figs 12A and B and 13A and B) and in lung cancer brain metastases (Supplementary Figs 12C and D and 13C and D) compared with corresponding normal tissues. Interestingly, the change of CCL2 expression in BM compared with normal brain was 2-fold higher than that of its primary counterpart, 1.2-fold for CCR2 and 20-fold for CCR4. Both astrocytes and microglia were found to be activated in the human and murine specimens of lung cancer brain metastases, indicated by GFAP and Iba1 markers, respectively (Supplementary Figs 12C and D and 13C and D).

The CCL2-CCR2/CCR4 axis is paramount to breast cancer cell proliferation, migration and invasion

To evaluate the role of CCL2 in the crosstalk between breast cancer cells and astrocytes, we performed proliferation, migration and 3D spheroid experiments in the presence of a CCL2 small molecular-weight inhibitor, bindarit. First, we performed proliferation assays of 4T1 and MDA-MB-231 cells, co-cultured with astrocytes or monocultured. In both cases, when the cells were treated with bindarit, breast cancer cell proliferation dramatically decreased, mainly in the co-cultures, returning it to a level similar to that in the monocultured cells not treated with the drug (Fig. 4A and B). A similar effect was achieved using a CCL2 neutralizing antibody (Supplementary Fig. 4A and B). In addition, using a Transwell migration assay, recombinant CCL2 protein (rCCL2) significantly increased MDA-MB-231 migration (Supplementary Fig. 4C), and the inhibition of CCL2 by bindarit significantly decreased MDA-MB-231 cell migration towards hAstro CM (Supplementary Fig. 4D). We further performed 3D tumour spheroids experiments, containing either breast cancer cells alone or breast cancer cells and astrocytes. When we treated the astrocyte-containing spheroids with bindarit, we observed a significant decrease in spheroid growth and sprouting (Fig. 4J–M). Similar results were obtained using CCL2 neutralizing antibody on astrocyte-containing MDA-MB-231 or EMT6 spheroids (Supplementary Fig. 4E and F).

We also created CCR4 knock-down cell lines using shRNA to inhibit this pathway molecularly and performed proliferation assays in the presence of astrocytes. 4T1 shCCR4 and MDA-MB-231 shCCR4 both presented a reduced proliferation rate when co-cultured with astrocytes (Fig. 4C and D). The shCCR4 cell proliferation rate was very similar in the presence or absence of astrocytes (Fig. 4C and D), confirming that the proliferation-promoting effect of the astrocytes on the breast cancer cells was mediated mainly by the CCL2 pathway.

Utilizing our BBB model, the inhibition of CCL2 by bindarit significantly increased the TEER values (Fig. 4H) and expression of the tight junction marker ZO1 (Fig. 4I), both indicating a tighter barrier. As expected, adding rCCL2 to the barrier decreased the TEER values (Fig. 4G), indicating a looser barrier. Moreover, rCCL2 treatment led to a more diffuse ZO1 pattern that relocated from the membrane to the cytoplasm (Fig. 4I).

Utilizing our lung cancer models, we observed increased proliferation of both human and murine lung cancer cells (A549 and LLC, respectively) in the presence of astrocytes, which was attenuated by the inhibition of CCL2 using bindarit (Supplementary Fig. 14A and B). A similar effect was detected using a 3D multicellular lung cancer brain metastases model (Supplementary Fig. 14C and D). Lastly, we utilized our lung cancer brain metastases mouse model for an efficacy study of bindarit. By inhibiting CCL2, bindarit led to a significant reduction in BM volume, measured by MRI, compared with the control group (Supplementary Fig. 15A and B).

P-selectin–P-selectin ligand-1 and PD-1–PD-L1 axes are upregulated in breast cancer brain metastasis

Most oncology protocols require combined therapies to allow synergistic activity, increase the therapeutic index of drugs with distinct mechanisms of action, improve toxicity profiles and prevent mechanisms of acquired resistance.[51] As we consider the CCL2-CCR2/CCR4 axis an immunological target, we rationally sought additional immune checkpoints to combine with CCL2 inhibition therapy. Therefore, we focused on the SELP–PSGL-1[11] and PD-1–PD-L1[52] axes.

We performed IHC staining on tissue sections, validating the expression of SELP and PSGL-1. We found both proteins were upregulated in BCBM compared with primary tumours and normal brain tissues, both in clinical samples and in our mouse model (Supplementary Fig. 5A–C). Further validation of patient data from the GSE12276 dataset[50] also showed a significantly increased expression of SELP and PSGL-1 in primary tumours that metastasized to the brain compared with tumours that metastasized to other organs (Fig. 5A and B).

We validated the expression of PD-1 and PD-L1 by IHC staining of the 4T1 BCBM mouse model. We found PD-1 and PD-L1 upregulated in BCBM compared with primary tumours and normal breast and brain tissues (Supplementary Fig. 5B and C). Validation of patient data from the GSE12276 dataset[50] confirmed that both PD-1 (significantly) and PD-L1 (non-significantly) present higher levels of expression in primary breast cancer tumours that have metastasized to the brain compared with breast cancer tumours that have metastasized to other organs (Fig. 5C and D).

The presence of SELP, PSGL-1, PD-1 and PD-L1 was further confirmed in BM of a spontaneous model of intracardially injected EMT6 cells (Supplementary Fig. 6).

Inhibition of CCL2 with SELP or PD-1/PD-L1 inhibition leads to improved outcomes versus monotherapy

Finally, we tested the inhibition of CCL2, SELP and PD-1/PD-L1 individually or combined, using three different models: (i) the 3D multicellular BCBM spheroid model; (ii) the 3D patient-derived metastatic breast cancer organoids co-cultured with bTME milieu; and (iii) the immunocompetent BALB/c mouse model.

As a human model for testing the drug combinations, we designed a unique 3D multicellular BCBM spheroid model, which is clinically relevant. This model enables us to explore immunotherapies, which is not possible with human cell lines or patient-derived xenografts (PDX) injected or implanted into mice, respectively, as these require immunocompromised animals. Therefore, we developed this additional model, which, unlike the model described earlier, is composed of breast cancer cells, astrocytes and microglia surrounded by PBMCs.

Prior to the *in vivo* studies utilizing this model, we found that the inhibition of either CCL2, SELP or PD-L1 individually as monotherapies reduced spheroid growth (Fig. 5E–G). The combination of CCL2 inhibitor with either PD-L1 inhibitor (PD-L1i) or SELP inhibitor (SELPi) led to a further reduction in spheroid growth (Fig. 5E–G).

As an additional model to test these combined therapies, we utilized patient-derived metastatic breast cancer 3D organoids and

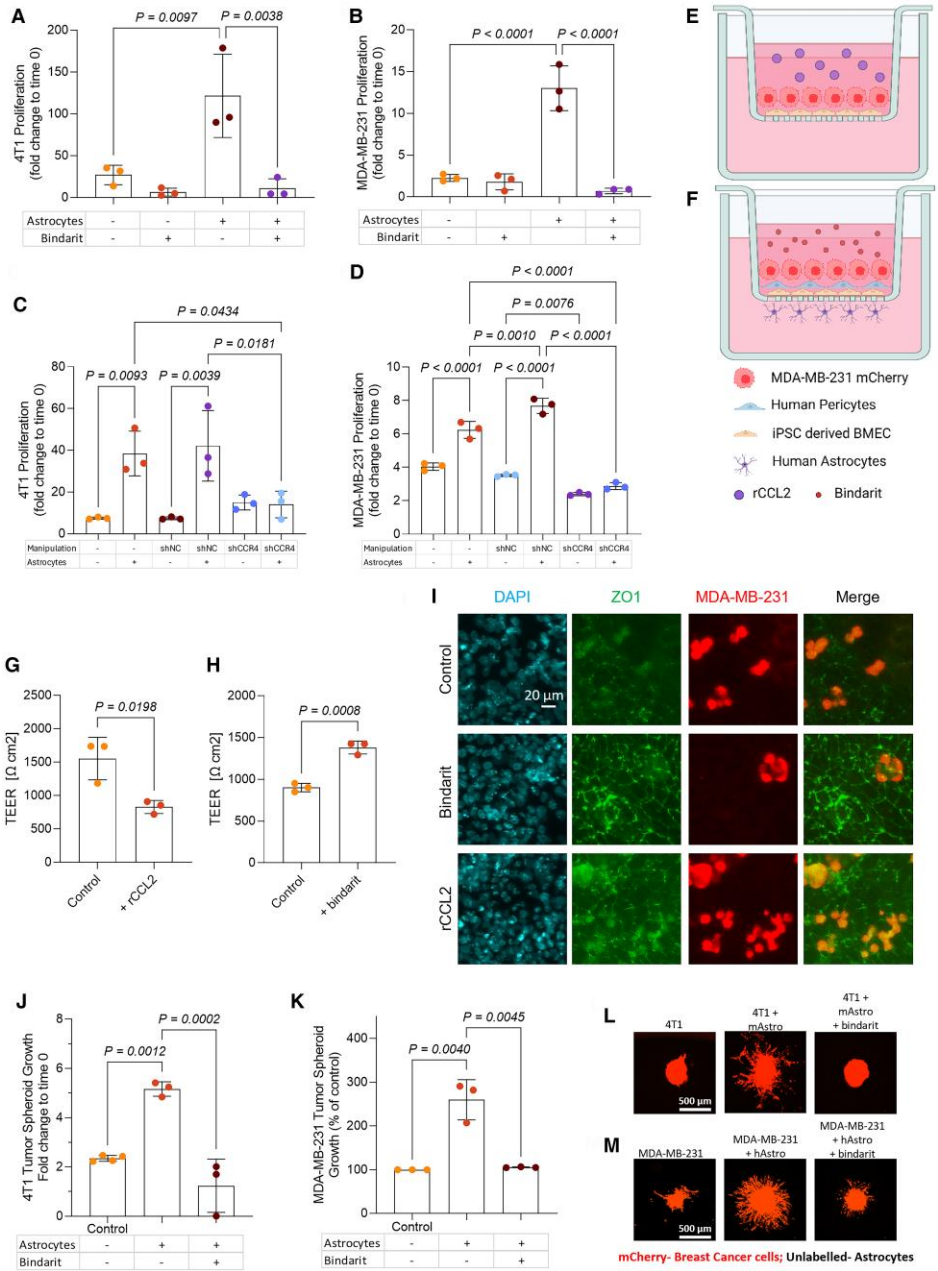

Figure 4 The CCL2–CCR2/CCR4 axis is important for breast cancer proliferation and invasion. (**A** and **B**) Proliferation rates after 160 h of (**A**) mCherry-labelled 4T1 cells in the presence or absence of murine astrocytes and CCL2 inhibitor bindarit ($n = 3$) and (**B**) mCherry-labelled MDA-MB-231 cells in the presence or absence of human astrocytes and CCL2 inhibitor bindarit ($n = 3$). Data are represented as fold-change to time 0. (**C** and **D**) Proliferation rates of (**C**) iRFP-labelled 4T1, shCCR4 or negative control sequence (shNC) cells in the presence or absence of murine astrocytes after 94 h (one representative of $n = 2$; dots on the graph represent technical repeats) and (**D**) iRFP-labelled MDA-MB-231, shCCR4 or shNC cells in the presence or absence of human astrocytes after 72 h (one representative of $n = 2$; dots on the graph represent technical repeats). Data are represented as fold-change to time 0. (**E** and **F**) Illustrations of the blood–brain barrier (BBB) models used in **G** and in **H** and **I** (respectively). This image was created with BioRender.com. (**G**) Trans-epithelial electrical resistance (TEER) values of a barrier consisting of induced pluripotent stem cell (iPSC)-derived brain microvascular endothelial cells (BMEC) and mCherry-labelled MDA-MB-231 cells, with or without the addition of recombinant CCL2 protein, measured 16 h after the addition of MDA-MB-231 cells ($n = 3$). Statistical significance was determined using an unpaired Student *t*-test. (**H**) TEER values of a barrier consisting of iPSC-derived BMEC, human pericytes, human astrocytes and mCherry-labelled MDA-MB-231 cells, with or without the addition of CCL2 inhibitor bindarit, measured 20 h after the addition of MDA-MB-231 cells ($n = 3$). Statistical significance was determined using an unpaired Student *t*-test. (**I**) Immunostaining of a barrier consisting of iPSC-derived BMEC, human pericytes, human astrocytes and mCherry-labelled MDA-MB-231 cells, with or without the addition of CCL2 inhibitor bindarit or recombinant CCL2 protein, measured 20 h after the addition of MDA-MB-231 cells. DAPI (cyan), tight junction marker ZO1 (green) and mCherry-labelled MDA-MB-231 cells (red). Scale bar = 20 µm. (**J** and **K**) Quantification of tumour spheroids area after 48 h of (**J**) mCherry-labelled 4T1 cells in the presence or absence of murine astrocytes and CCL2 inhibitor bindarit (one representative of $n = 2$; dots on the graph represent technical repeats, data are presented as fold-change to time 0) and (**K**) mCherry-labelled MDA-MB-231 cells in the presence or absence of human astrocytes and CCL2 inhibitor bindarit ($n = 3$) (data are presented as % of control). (**L** and **M**) Representative images of tumour spheroids from **J** and **K** (respectively). Scale bars = 500 µm. All data are expressed as mean ± standard deviation. Unless otherwise stated, statistical significance was determined using one-way ANOVA and Tukey's multiple comparisons tests. mAstro = murine astrocytes; hAstro = human astrocytes.

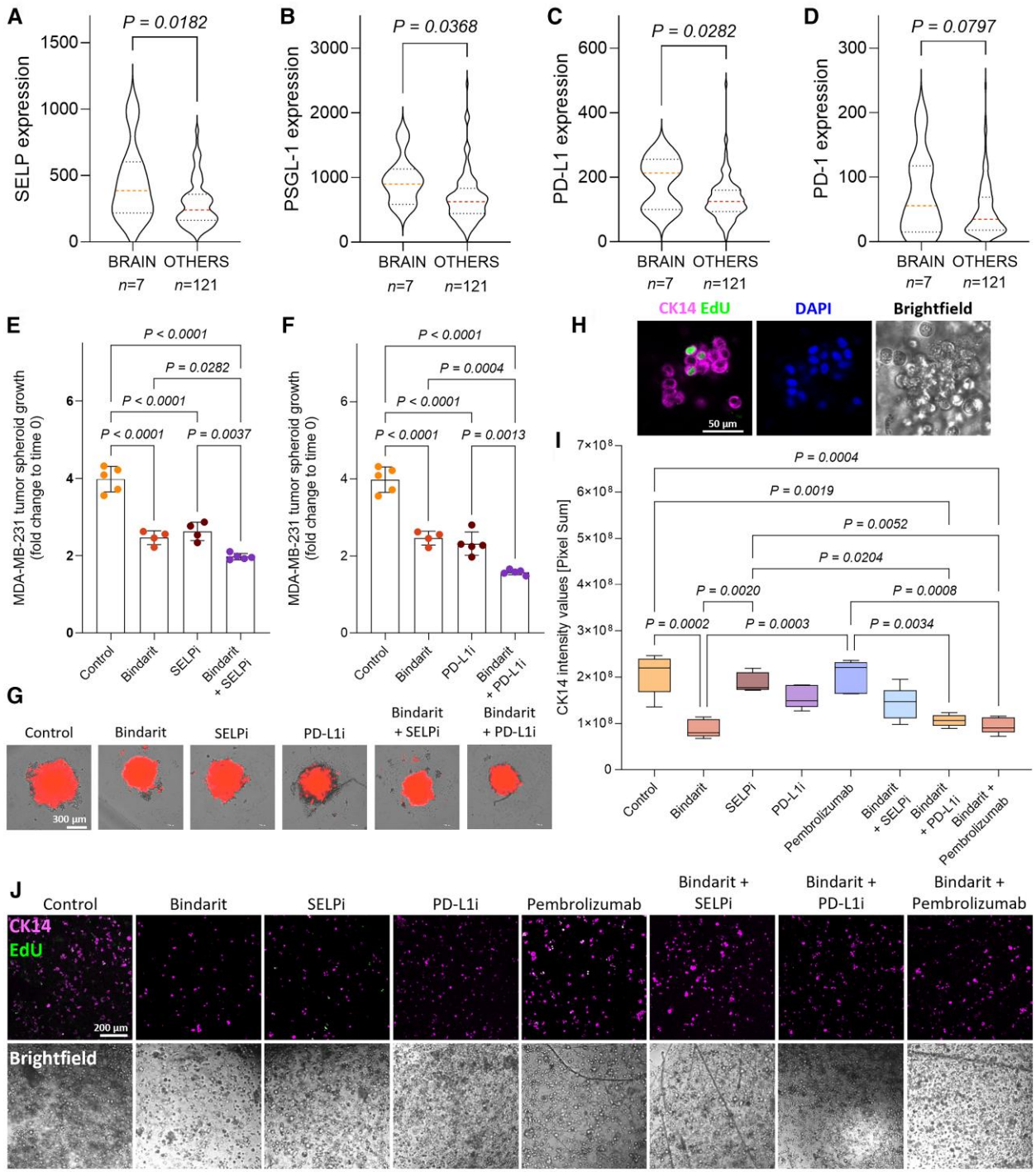

Figure 5 P-selectin–P-selectin ligand and PD-1–PD-L1 axes are promising candidates for immunotherapeutic combination therapy together with CCL2 inhibition. (**A–D**) mRNA expression analysis of (**A**) P-selectin (SELP), (**B**) P-selectin ligand 1 (PSGL-1), (**C**) Programmed death-ligand 1 (PD-L1) and (**D**) Programmed cell death protein 1 (PD-1) on human primary breast tumours that metastasized to the brain, compared with those that metastasized to other organs (data from GSE12276). Data are presented as violin plots, showing the median and quartiles. Statistical significance was determined using a one-tailed non-paired Student's *t*-test. (**E** and **F**) Quantification of tumour spheroids area after 120 h of mCherry-labelled MDA-MB-231 cells in the presence of human astrocytes, human microglia and peripheral blood mononuclear cells (PBMCs) treated with (**E**) bindarit and/or SELPi (one representative of $n = 3$; dots on the graph represent technical repeats) and (**F**) bindarit and/or PD-L1i ($n = 4–5$). Data are expressed as mean ± standard deviation. Statistical significance was determined using one-way ANOVA and Tukey's multiple comparisons tests. (**G**) Representative images of spheroids from **E** and **F**. Scale bar = 300 µm. (**H–J**) Patient-derived breast cancer liver metastasis organoids co-cultured with human astrocytes, human microglia and PBMCs treated with bindarit and/or SELPi, PD-L1i and Pembrolizumab. (**H**) Confocal imaging of a representative control organoid stained for CK14 antibody (magenta), EdU-based proliferation marker (green) and DAPI (blue). Scale bar = 50 µm. (**I**) Quantification of CK14 intensity of immunostained organoids ($n = 5$ fields for each group). Data are presented as a box-and-whisker plot, with a line at the median and an error bar representing minimal and maximal values. Statistical significance was determined using one-way ANOVA and Tukey's multiple comparisons tests. (**J**) Representative confocal images of the CK14 quantified organoids from **H**. CK14 (magenta), EdU-based proliferation marker (green). Scale bar = 200 µm. PD-L1i = programmed death-ligand 1 inhibitor; SELPi = p-selectin inhibitor.

cultured them with astrocytes, microglia and PBMCs. By immunostaining the organoids with Cytokeratin 14 (CK14) as a marker for breast cancer cells, we were able to quantify the effect of the treatments on organoid growth (Fig. 5H–J and Supplementary Fig. 7). The analysis

revealed that the organoids were highly sensitive to the treatment with bindarit as a monotherapy (Fig. 5I and J). We further treated this model with SELPi, PD-L1i and the clinically used αPD-1 antibody, Pembrolizumab. The effect of combining bindarit with any of these three drugs was better than that of each drug individually, although not superior to bindarit alone (Fig. 5I and J).

To model the disease course *in vivo* as closely as possible to the human disease in which metastases develop after a primary tumour is established, 4T1 cells were first inoculated orthotopically into the mammary fat pad, and tumours were later resected. The existence of a primary tumour is also necessary to achieve an intracranial response to immune checkpoint inhibitors (ICIs), as previously shown in a melanoma BM model.[53] To ensure that no metastases were present at the stage in which we removed the primary tumour, the resections were done when the primary tumours were very small (<50 mm^3) and unlikely to have metastasized. The tumours had well-defined edges and were removed whole, as shown by haematoxylin and eosin staining (Supplementary Fig. 8). To evaluate the effect of the anti-cancer drugs on metastasis progression, a model with 100% brain metastases development was required to allow for follow-up and monitoring using MRI. Thus, following the primary tumour resection, 4T1 cells were injected intracranially, and mice were treated with CCL2 inhibitor bindarit, SELPi and αPD-1 antibody for 2 weeks. The experimental time course and treatment regimen are detailed in Fig. 6A.

Each drug significantly increased overall survival (OS) in mice compared with the control group. Combining bindarit with either of the other targets led to a further increase in OS (Fig. 6B and C). Analysis of systemic disease relapse, presented by primary tumour recurrence or detection of extracranial metastases, revealed another advantage of the combination therapies. While bindarit and SELPi individually did not lead to any improvement in relapse in comparison with the control group, the combination of these drugs led to a delay in the detection of any relapse and a decrease in the overall percentage of mice presenting extracranial metastases or tumour recurrence (Fig. 6D). In the case of the ICI, αPD-1 antibody had a better profile in terms of relapse compared to the control group, and when combined with bindarit, this improved even further (Fig. 6E). These findings suggested that drug combinations with inhibitors of the CCL2–CCR2/CCR4 axis may impede recurrence and extracranial metastases besides the BM.

No additional toxicities were detected due to the combination of two drugs, either in body-weight changes (Fig. 6H) or blood chemical and haematological tests (Supplementary Figs 9 and 10).

Each drug alone significantly decreased the BM volume and both drug combinations resulted in a slight, non-significant improvement compared with each monotherapy (Fig. 6F and G).

Mice brain tissues were collected and further analysed by IHC staining (Fig. 7 and Supplementary Fig. 11). The analysis revealed that all treatments led to lower CCL2, CCR2 and CCR4 levels, indicating decreased inflammation. In addition, the inhibition of proliferation was observed as indicated by the proliferation marker Ki-67 and increased apoptosis as indicated by the Caspase-3 marker. Blood vessel density was strongly reduced by bindarit, and an even further reduction was presented following the combination treatments, as indicated by the CD31 marker. As expected, CD8+ cytotoxic T-lymphocyte infiltration was increased by the monotherapies and the combination therapies. The expression of CD4+ T helper cells did not change significantly between the groups. The presence of FOXP3+ regulatory T cells (Treg) was slightly decreased by all treatments (non-significantly), and the combination of bindarit and αPD-1 treatment presented lower levels of Treg cells. The expression levels of PD-L1 were reduced when the mice were treated with either SELPi, αPD-1 antibody or the drug combinations. This could be due to an effect of the drugs on antigen-presenting cells (APC), such as dendritic cells or macrophages, pushing them towards a pro-inflammatory M1-like phenotype. The reduced PD-L1 expression and pro-inflammatory activation of myeloid cells led to a reduction in their immunosuppressive effect on the cytotoxic T cells, resulting in a lower expression of PD-1.

Discussion

CCL2 is a critical proinflammatory cytokine in cancer, as it mediates the signalling of both CCR2 and CCR4.[54] Therefore, this signalling axis has drawn considerable attention in cancer research.[54-59] Largely, previous studies have focused either on the correlation of CCL2 expression with breast cancer histological grade[60] or on its important role as a regulator of angiogenesis and immune cell recruitment.[61-63] Moreover, CCL2 has been further shown to promote extracranial metastasis by supporting breast cancer cell proliferation, survival, migration and invasion.[64-69] However, the pro-metastatic effects of the bTME induced by astrocyte-secreted CCL2 are mostly unknown.

We have characterized the mutual effects of astrocytes and breast cancer cells in co-cultures and in the presence of CM, mimicking the settings in the different steps of metastases formation, from distant communication to physical interactions. Our findings confirm a reciprocal activation of astrocytes and breast cancer cells, suggesting that reactive astrocytes can remotely facilitate breast cancer cell migration. We developed an additional model for mimicking the clinical scenario, in which breast cancer cells extravasate from the bloodstream into the brain through the BBB, demonstrated by the trans-endothelial and trans-astrocytic passage towards astrocyte-secreted cytokines. This model also revealed that even without physical interactions, astrocytes enhanced breast cancer cell penetration through the BBB model. Once the breast cancer cells penetrate the brain parenchyma, their proliferation and invasiveness are induced by astrocytes. Collectively, our results suggest that astrocytes have a supportive role in the metastatic process of breast cancer in the brain.

We further identified some cytokines as candidates involved in breast cancer cell–bTME interactions. The leading candidate was CCL2, which was not only found to be overexpressed in co-cultures of breast cancer cells and astrocytes but also highly relevant in clinical samples, as we showed that it was overexpressed in BM compared to primary tumours and normal breast and brain tissues.

Cancer and stromal cells in the tumour microenvironment can produce CCL2, which affects cancer cells directly and indirectly by the recruitment of pro-tumourigenic host stromal cells during metastasis [including, among others, tumour-associated macrophages (TAMs), Tregs and myeloid-derived suppressor cells (MDSCs)].[37,54,70,71] The stromal expression of CCL2 was found to correlate with relapse-free survival.[72] The receptors that are known to bind CCL2 are CCR2 and CCR4. CCR2 expression was found to promote the recruitment of TAMs at the primary tumour and enhance invasion, angiogenesis and extracranial metastasis of breast cancer.[70] CCR4 expression has a strong correlation to lower overall

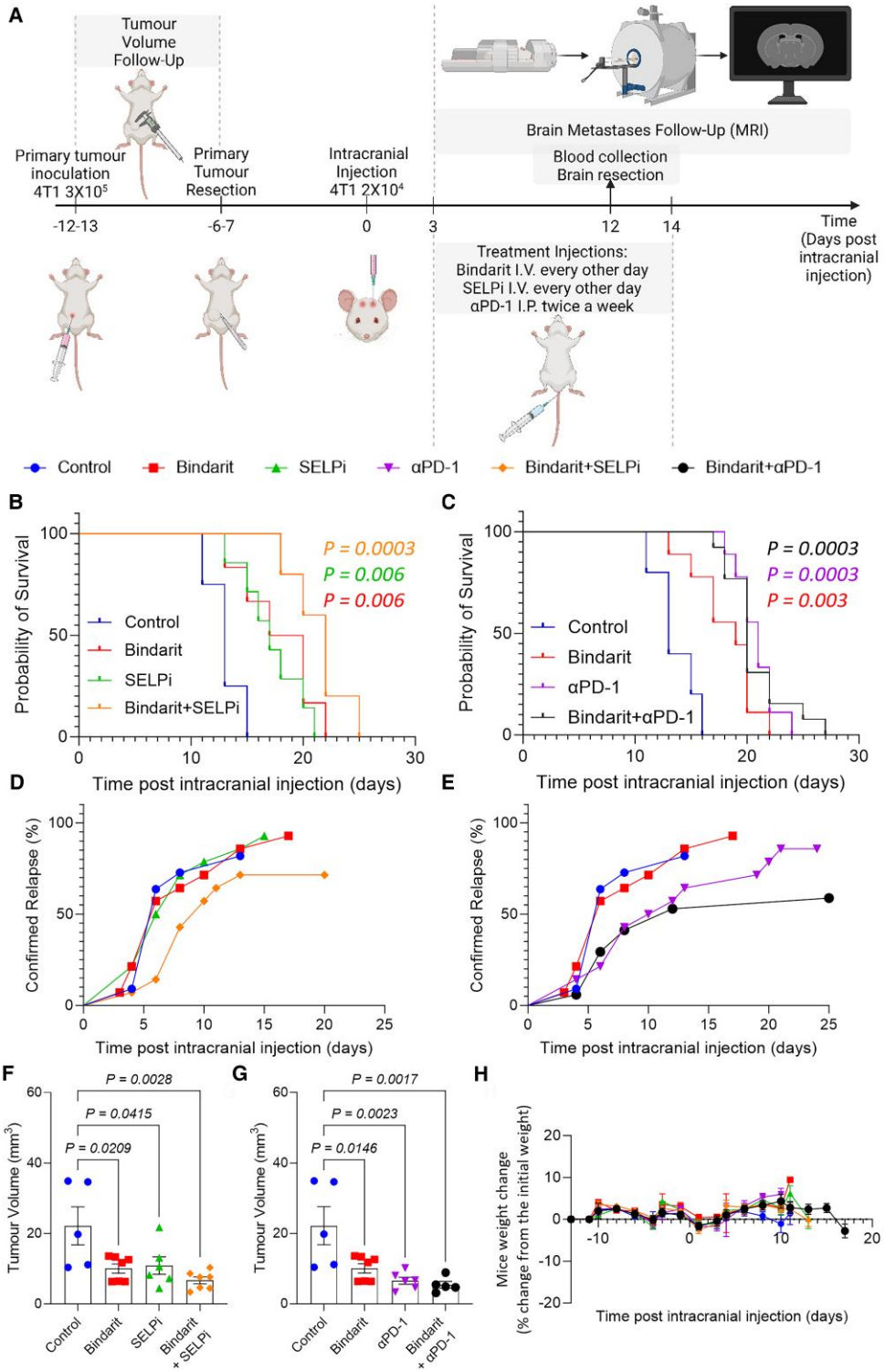

Figure 6 Combination therapy of bindarit and either P-selectin inhibitor or αPD-1 antibody leads to favourable outcomes in orthotopic breast cancer brain metastases mouse model. (**A**) Timeline (days) of primary tumour inoculation, tumour resection, metastases induction (intracranial injection), treatments and follow-up. (**B** and **C**) Kaplan–Meier survival curves of the different treatment groups. Statistical significance was determined using a survival analysis of each group compared to the control group, with further adjustment of *P*-values using a Holm–Šídák analysis. Number of mice for survival analysis: control $n = 4$, bindarit $n = 6$, SELPi $n = 7$, αPD-1 $n = 6$, bindarit + SELPi $n = 5$, bindarit + αPD-1 $n = 6$. (**D** and **E**) Primary tumour recurrence and extracranial metastases development inhibition are presented as the kinetics of development over time within the groups. Number of mice for relapse analysis: control $n = 11$, bindarit $n = 14$, SELPi $n = 14$, αPD-1 $n = 14$, bindarit + SELPi $n = 14$, bindarit + αPD-1 $n = 17$. (**F** and **G**) Quantification of brain metastases size 10 days post intracranial injection. Data are expressed as mean ± standard error of the mean; statistical significance was determined using one-way ANOVA and Tukey's multiple comparisons tests. Number of mice for tumour volume analysis: control $n = 5$, bindarit $n = 7$, SELPi $n = 6$, αPD-1 $n = 6$, bindarit + SELPi $n = 7$, bindarit + αPD-1 $n = 5$. (**H**) Body weight change is presented as the % of change compared with the initial weight prior to primary tumour inoculation. Data are expressed as mean ± standard error of the mean. αPD-1 = anti-programmed death-1 antibody; SELPi = P-selectin inhibitor.

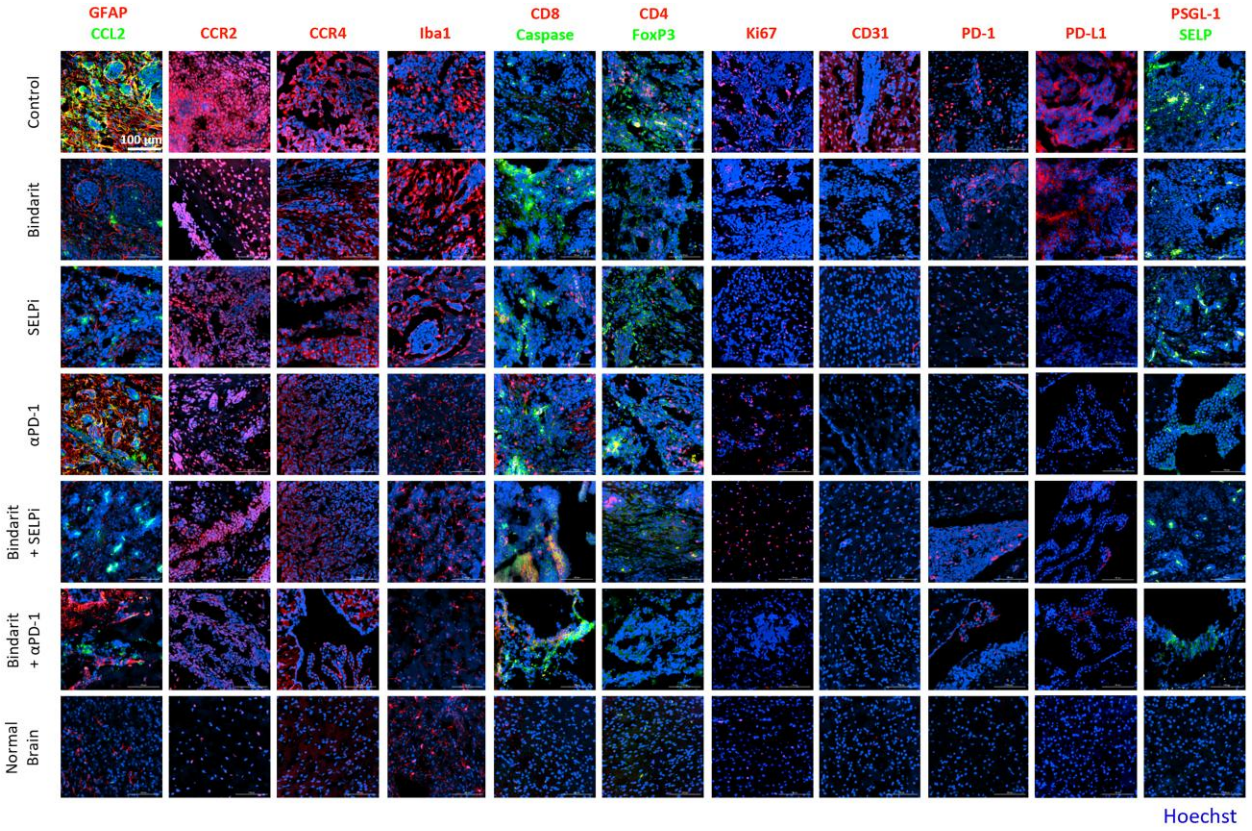

Figure 7 Combination therapy of bindarit and either P-selectin inhibitor or αPD-1 antibody leads to reduced tumour proliferation, increased immune activation and reduced immune suppression. GFAP (red) + CCL2 (green), CCR2 (red), CCR4 (red), Iba1 (red), CD8 (red) + Caspase 3 (green), Ki67 (red), CD31 (red), PD-1 (red), PD-L1 (red), PSGL-1 (red) + SELP (green), Hoechst (blue) staining in brain metastases tissue sections from control and treated mice. Scale bars = 100 µm. Representative images of selected fields. αPD-1 = anti-programmed death-1 antibody; SELPi = p-selectin inhibitor.

survival in breast cancer patients and also positively correlates with tumour recurrence and lymph node, lung and bone metastases.[71] As far as we know, prior to our publication regarding melanoma BM, the key role of the CCL2–CCR2/CCR4 axis had not been demonstrated in the context of astrocyte–cancer cell crosstalk.[14]

We now show that the main source of secreted CCL2 in BCBM is the activated astrocytes that support the tumourigenic properties of cancer cells. The breast cancer cells, in turn, increase the expression of CCR2 and CCR4. When we functionally neutralized the CCL2–CCR2/CCR4 axis, either pharmacologically or molecularly, BCBM cell proliferation, migration and invasion rates decreased, and BBB integrity improved. To the best of our knowledge, this is the first report demonstrating that activated astrocytes play a key role in BCBM *via* secretion of CCL2 interacting with CCR2 and CCR4 on the surface of breast cancer cells.

We are suggesting that the CCL2 pathway is important for the metastatic colonization process in the brain in general and is not limited to breast cancer only. To strengthen the evidence supporting our hypothesis, we also show the contribution of the CCL2–CCR2/CCR4 axis to lung cancer BM in several models. As we previously established the importance of this axis in the context of melanoma BM[14] and now show evidence of its role in BCBM and lung cancer BM, we suggest that the CCL2–CCR2/CCR4 axis is a key pathway in the brain metastatic cascade arising from the leading three primary tumour sites metastasizing to the brain.[5] We further propose that the CCL2 pathway plays a key role in astrocyte–cancer cell signalling during BM formation. We hypothesize that this is an interesting phenomenon, where different types of cancer cells arising from different origins and locations may share a common signalling pathway to interact with astrocytes and lead to brain metastases colonization, establishment and progression.

As BM are highly aggressive, monotherapy is usually ineffective, and tumour resistance mechanisms can elicit disease relapse.[73] Specifically, CCL2 inhibition in metastatic breast cancer mouse models has been reported to increase metastatic relapse after cessation of treatment.[74] Therefore, we searched for additional targets to combine with CCL2 inhibition and sought targets involved in interactions with additional bTME components.

We previously reported the expression of SELP on glioblastoma cells to modulate the activation state of microglia and influence T-cell recruitment.[11] We further characterized the P-selectin–P-selectin ligand-1 axis as a key regulator of the crosstalk between glioblastoma and microglial cells and demonstrated a potential therapeutic approach for glioblastoma.[11] The inhibition of SELP led to reduced tumour growth and increased survival in glioblastoma mouse models.[11]

ICIs targeting PD-1 or its ligand PD-L1 have demonstrated intracranial effects in brain metastases originating from melanoma and NSCLC.[39,40] In comparison to melanoma, NSCLC and other malignancies, breast cancer has traditionally been considered immunologically cold, with relatively low levels of T-cell infiltration and mutational burdens.[75] More recently, the immune system involvement in breast cancer progression, response to treatment and development of resistance have begun to be re-evaluated, opening the door to immunotherapeutic approaches.[38] In a recently published study, ICIs showed promise in treating metastatic breast

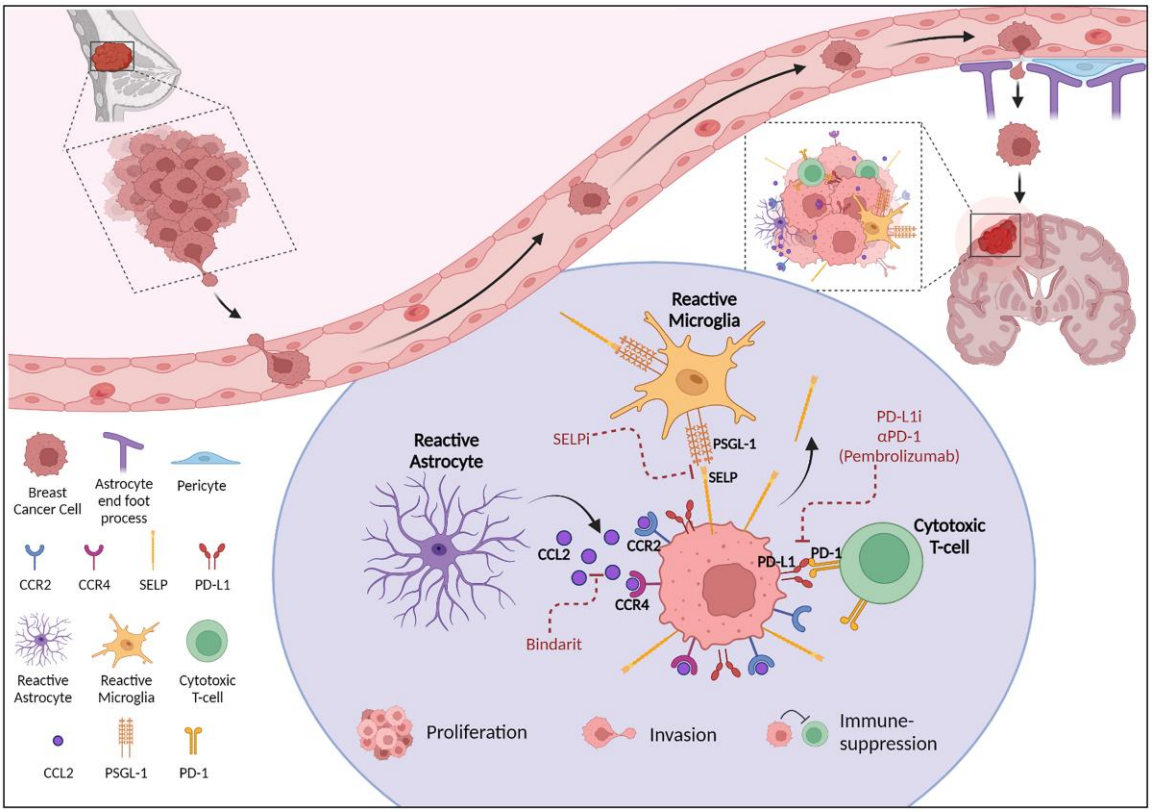

Figure 8 Summary model. Illustration showing proposed immunotherapeutic combination approach—inhibiting breast cancer brain metastases interactions with the brain milieu. Inhibition of the three axes CCL2–CCR2/CCR4, SELP–PSGL-1 and PD-1–PD-L1 can prevent breast cancer brain metastases progression. By combining these treatments, favourable long-term effects could be achieved. This image was created with BioRender.com.

cancer.[76] However, there is a lack of data regarding their efficacy in breast cancer patients with BM, as these are often excluded from clinical trials due to concerns regarding toxicities, limited efficacy of systemic agents crossing the BBB and overall poor prognosis.[76,77]

To evaluate the relevance of the SELP–PSGL-1 and PD-1–PD-L1 axes to BCBM patients, we performed a gene expression analysis of the GSE12276 dataset,[50] which revealed that these were overexpressed in primary tumours that relapsed in the brain, in comparison to tumours that metastasized to other organs. Additionally, IHC staining of tissue sections obtained from patients and our mouse models revealed that SELP, PSGL-1, PD-1 and PD-L1 are upregulated in BCBM. In light of that, we propose these two axes as potential candidates in combination with CCL2 inhibition.

We further show that the combination of a CCL2 inhibitor with these other two immunological checkpoints is beneficial. We demonstrated this using two independent techniques: (i) syngeneic mouse models of BCBM mice; and (ii) different 3D multicellular tumouroid models.

When we tested these combinations *in vivo*, treatment with CCL2 inhibitor, together with either SELP inhibitor or αPD-1 antibody, led to modest improvement in some parameters compared to the monotherapies. Both combinations demonstrated an increase in OS and a slight reduction in BM volume compared with the relevant monotherapies and a systemic effect, leading to a reduction in primary tumour recurrence and reduced presentation of additional extracranial metastatic sites. As this mouse model is highly aggressive, with very large BM lesions, the most meaningful effect, which was achieved by combining CCL2 inhibitor with αPD-1 antibody, prolonged the survival of mice in approximately 1 week, compared to the control group. Although the combined therapies resulted in modest improvement of some aspects of disease progression, we suggest these targets as potential combined therapy options. Future research should involve 3D *in vitro* models and mouse models of earlier stages of micro-metastases formation, which could enable earlier intervention and even better survival outcomes. This would also allow for the investigation of the cancer cell-secreted factors that initiate the activation of astrocytes in the first place and lead to the cascade of events described here.

We also tested these combined immunomodulation therapies in different 3D models, in which the drug combinations showed a modest improvement compared with the monotherapies. In summary, due to the increased efficacy of targeting multiple axes simultaneously, and the potential to reduce the incidence of acquired drug resistance (not tested), we suggest that the combination of CCL2 inhibition with (i) SELP inhibition or (ii) PD-1/PD-L1 inhibition, may, following further investigation, provide promising immunotherapeutic approaches.

Throughout the study, we utilized our 3D multicellular BCBM tumour models, using two of the most common methods for the fabrication of multicellular tumour spheroids[44]: (i) the hanging drop; and (ii) the liquid overlay technique. Recently, the US Food and Drug Administration Modernization Act 2.0 was approved, aiming to reduce animal experimentation and promote the development of more accurate *in vitro* models based on human cells to better assess products for human application.[78] Compared with traditional 2D cell culture models, 3D models composed of cancer cells and components of the tumour microenvironment better mimic solid tumours in terms of their architecture and phenotypic features.[44,79,80] 2D *in*

vitro models do not fully represent the cellular and functional complexities of tumours,[81] and animal models are not only ethically controversial but also limited with regard to clinically relevant responses to treatments, especially when immunotherapies are considered.[82,83] Thus, 3D models may assist in closing the gap between traditional *in vitro* and *in vivo* studies and human clinical trials.[44]

Throughout the different steps of our study, by utilizing different 3D models, we revealed similar results regarding the effects of astrocytes on breast cancer cells, as well as results that support the functional involvement of CCL2 in this intercommunication, while comparing the data with findings that originated from clinical samples. In addition to cancer cells, we incorporated multiple cell populations in these models, including astrocytes, endothelial cells, microglia and PBMCs, thus better mimicking the bTME. This allowed us to perform complex studies with drugs that target not only cancer cells but also their microenvironment, with great implications for therapeutic options in humans. As an additional 3D model, we used patient-derived metastatic breast cancer organoids, which we co-cultured with bTME components and later treated with the drug combinations.

In summary, we demonstrate a previously unidentified and unique requirement for the CCL2–CCR2/CCR4 axis in the crosstalk between breast cancer cells and astrocytes during breast cancer metastatic cascades in the brain. These data provide a new understanding of the signalling mechanisms required for brain colonization and metastatic progression. As detailed in Fig. 8, our findings implicate astrocyte-secreted CCL2 as a necessary component of the complex signalling network in brain metastasis, corroborating with proinflammatory cytokines expressed on multiple immune cells such as P-selectin on microglia/TAMs and PD-1 on T cells, presenting a unique prophylactic and therapeutic immunotherapeutic approach for BCBM following resection of the primary lesion.

Data availability

The authors confirm that the data supporting the findings of this study are available within the article and its Supplementary material.

Acknowledgements

S.I.D. was a TEVA BioInnovation fellow in advanced research.

Funding

R.S.-F. received partial funding from the European Research Council (ERC) Advanced Grant (835227; 3DBrainStrom); and ERC Proof of Concept (PoC) Grant (862580; 3DCanPredict); The Israel Science Foundation (1969/18); The Israel Cancer Research Fund (PROF-18-682); the Morris Kahn Foundation; and "La Caixa" Foundation under the framework of the Healthcare Research call 2022 (LCF/PR/HR22/52420016; MultiNano@BBM).

Competing interests

H.B. is a consultant for AsclepiX Therapeutics, Perosphere Inc./AMAG Pharmaceuticals, Inc., StemGen, InSightec, Accelerating Combination Therapies, Camden Partners, LikeMinds, Inc., Galen Robotics, Inc., Nurami Medical and B*CURED. J.B.: Advisor: AbbVie, Amgen, AstraZeneca, Bayer, MSD, Merck-Serono, Roche, Takeda; Writing/speaker engagement: BMS, Medison, Pfizer. Research funding: Immunai, OncoHost, MSD, AstraZeneca, Roche, Abbvie. R.S.-F. is a board director at Teva Pharmaceutical Industries Ltd. and receives unrelated research funding from Merck KGaA. All other authors report no competing interests.

Supplementary material

Supplementary material is available at *Brain* online.

References

1. Sung H, Ferlay J, Siegel RL, et al. Global cancer statistics 2020: GLOBOCAN estimates of incidence and mortality worldwide for 36 cancers in 185 countries. *CA Cancer J Clin*. 2021;71:209-249.
2. Siegel RL, Miller KD, Wagle NS, Jemal A. Cancer statistics, 2023. *CA Cancer J Clin*. 2023;73:17-48.
3. Jandial R, Hoshide R, Waters JD, Somlo G. Operative and therapeutic advancements in breast cancer metastases to the brain. *Clin Breast Cancer*. 2018;18:e455-e467.
4. Custodio-Santos T, Videira M, Brito MA. Brain metastasization of breast cancer. *Biochim Biophys Acta Rev Cancer*. 2017;1868:132-147.
5. Doron H, Pukrop T, Erez N. A blazing landscape: Neuroinflammation shapes brain metastasis. *Cancer Res*. 2019; 79:423-436.
6. Witzel I, Oliveira-Ferrer L, Pantel K, Müller V, Wikman H. Breast cancer brain metastases: Biology and new clinical perspectives. *Breast Cancer Res*. 2016;18:1-9.
7. Rostami R, Mittal S, Rostami P, Tavassoli F, Jabbari B. Brain metastasis in breast cancer: A comprehensive literature review. *J Neurooncol*. 2016;127:407-414.
8. Leone JP, Leone BA. Breast cancer brain metastases: The last frontier. *Exp Hematol Oncol*. 2015;4:33.
9. Joyce JA, Pollard JW. Microenvironmental regulation of metastasis. *Nat Rev Cancer*. 2009;9:239-252.
10. Albini A, Sporn MB. The tumour microenvironment as a target for chemoprevention. *Nat Rev Cancer*. 2007;7:139-147.
11. Yeini E, Ofek P, Pozzi S, et al. P-selectin axis plays a key role in microglia immunophenotype and glioblastoma progression. *Nat Commun*. 2021;12:1-22.
12. Schwartz H, Blacher E, Amer M, et al. Incipient melanoma brain metastases instigate astrogliosis and neuroinflammation. *Cancer Res*. 2016;76:4359-4371.
13. Valiente M, Ahluwalia MS, Boire A, et al. The evolving landscape of brain metastasis. *Trends Cancer*. 2018;4:176-196.
14. Pozzi S, Scomparin A, Ben-Shushan D, et al. MCP-1/CCR2 axis inhibition sensitizes the brain microenvironment against melanoma brain metastasis progression. *JCI insight*. 2022;7:e154804.
15. Wu S, Lu J, Zhu H, et al. A novel axis of circKIF4A-miR-637-STAT3 promotes brain metastasis in triple-negative breast cancer. *Cancer Lett*. 2024;581:216508.
16. Ferraro GB, Ali A, Luengo A, et al. Fatty acid synthesis is required for breast cancer brain metastasis. *Nat Cancer*. 2021;2:414-428.
17. Cicero J, Trouvilliez S, Palma M, et al. ProNGF promotes brain metastasis through TrkA/EphA2 induced Src activation in triple negative breast cancer cells. *Exp Hematol Oncol*. 2023;12:104.
18. Adler O, Zait Y, Cohen N, et al. Reciprocal interactions between innate immune cells and astrocytes facilitate neuroinflammation and brain metastasis via lipocalin-2. *Nat Cancer*. 2023;4: 401-418.
19. Xie J, Yang A, Liu Q, et al. Single-cell RNA sequencing elucidated the landscape of breast cancer brain metastases and identified ILF2 as a potential therapeutic target. *Cell Prolif*. 2024;57:e13697.

20. Zou Y, Ye F, Kong Y, et al. The single-cell landscape of intratumoral heterogeneity and the immunosuppressive microenvironment in liver and brain metastases of breast cancer. *Advanced Science*. 2023;10:2203699.
21. Rodrigues G, Hoshino A, Kenific CM, et al. Tumour exosomal CEMIP protein promotes cancer cell colonization in brain metastasis. *Nat Cell Biol*. 2019;21:1403-1412.
22. Nicolson G, Menter D, Herrmann J, Yun Z, Cavanaugh P, Marchetti D. Brain metastasis: Role of trophic, autocrine, and paracrine factors in tumor invasion and colonization of the central nervous system. *Curr Top Microbiol Immunol*. 1996;213:89-115.
23. Fitzgerald DP, Palmieri D, Hua E, et al. Reactive glia are recruited by highly proliferative brain metastases of breast cancer and promote tumor cell colonization. *Clin Exp Metastasis*. 2008;25:799-810.
24. Zhang M, Olsson Y. Hematogenous metastases of the human brain–characteristics of peritumoral brain changes: A review. *J Neurooncol*. 1997;35:81-89.
25. Priego N, Zhu L, Monteiro C, et al. STAT3 labels a subpopulation of reactive astrocytes required for brain metastasis. *Nat Med*. 2018;24:1024-1035.
26. Termini J, Neman J, Jandial R. Role of the neural niche in brain metastatic cancer. *Cancer Res*. 2014;74:4011-4015.
27. Lorger M, Felding-Habermann B. Capturing changes in the brain microenvironment during initial steps of breast cancer brain metastasis. *Am J Pathol*. 2010;176:2958-2971.
28. Klein A, Schwartz H, Sagi-Assif O, et al. Astrocytes facilitate melanoma brain metastasis via secretion of IL-23. *J Pathol*. 2015;236:116-127.
29. Daginakatte GC, Gutmann DH. Neurofibromatosis-1 (Nf1) heterozygous brain microglia elaborate paracrine factors that promote Nf1-deficient astrocyte and glioma growth. *Hum Mol Genet*. 2007;16:1098-1112.
30. He BP, Wang JJ, Zhang X, et al. Differential reactions of microglia to brain metastasis of lung cancer. *Mol Med*. 2006;12:161.
31. Hoelzinger DB, Demuth T, Berens ME. Autocrine factors that sustain glioma invasion and paracrine biology in the brain microenvironment. *J Natl Cancer Inst*. 2007;99:1583-1593.
32. Roggendorf W, Strupp S, Paulus W. Distribution and characterization of microglia/macrophages in human brain tumors. *Acta Neuropathol*. 1996;92:288-293.
33. Markovic DS, Glass R, Synowitz M, Nv R, Kettenmann H. Microglia stimulate the invasiveness of glioma cells by increasing the activity of metalloprotease-2. *J Neuropathol Exp Neurol*. 2005;64:754-762.
34. Markovic D, Vinnakota K, Chirasani S, et al. Gliomas induce and exploit microglial MT1-MMP expression for tumor expansion. *Proc Natl Acad Sci*. 2009;106:12530-12535.
35. Ji M, Ricciardi-Castagnoli P, Mange PDLE, Martin F, Juilleratt-Jeanneret L. Microglial cells induce cytotoxic effects toward colon carcinoma cells: Measurement of tumor cytotoxicity with a γ-glutamyl transpeptidase assay. *Int J Cancer*. 1997;70:169-174.
36. Rollins BJ. Chemokines. *Blood*. 1997;90:909-928.
37. Marcuzzi E, Angioni R, Molon B, Calì B. Chemokines and chemokine receptors: Orchestrating tumor metastasization. *Int J Mol Sci*. 2019;20:96.
38. Emens LA, Adams S, Cimino-Mathews A, et al. Society for Immunotherapy of Cancer (SITC) clinical practice guideline on immunotherapy for the treatment of breast cancer. *J Immunother Cancer*. 2021;9:e002597.
39. Goldberg SB, Schalper KA, Gettinger SN, et al. Pembrolizumab for management of patients with NSCLC and brain metastases: Long-term results and biomarker analysis from a non-randomised, open-label, phase 2 trial. *Lancet Oncol*. 2020;21:655-663.
40. Tawbi HA, Forsyth PA, Algazi A, et al. Combined nivolumab and ipilimumab in melanoma metastatic to the brain. *N Engl J Med*. 2018;379:722-730.
41. Ferber S, Tiram G, Sousa-Herves A, et al. Co-targeting the tumor endothelium and P-selectin-expressing glioblastoma cells leads to a remarkable therapeutic outcome. *Elife*. 2017;6:e25281.
42. Rauti R, Ess A, Le Roi B, et al. Transforming a well into a chip: A modular 3D-printed microfluidic chip. *APL Bioeng*. 2021;5:026103.
43. Sade O, Boneberg R, Weiss Y, et al. Super-Resolution-Chip: An in-vitro platform that enables super-resolution microscopy of co-cultures and 3D systems. *Biomed Opt Express*. 2023;14:5223-5237.
44. Pozzi S, Scomparin A, Israeli Dangoor S, et al. Meet me halfway: Are in vitro 3D cancer models on the way to replace in vivo models for nanomedicine development? *Adv Drug Deliv Rev*. 2021;175:113760.
45. Rauh U, Wei G, Serrano-Wu M, et al. BRD-810 is a highly selective MCL1 inhibitor with optimized in vivo clearance and robust efficacy in solid and hematological tumor models. *Nat Cancer*. 2024;5:1479–1493.
46. Parida PK, Marquez-Palencia M, Ghosh S, et al. Limiting mitochondrial plasticity by targeting DRP1 induces metabolic reprogramming and reduces breast cancer brain metastases. *Nat Cancer*. 2023;4:893-907.
47. Sun X, Tang H, Chen Y, et al. Loss of the receptors ER, PR and HER2 promotes USP15-dependent stabilization of PARP1 in triple-negative breast cancer. *Nat Cancer*. 2023;4:716-733.
48. Wang L, Cossette SM, Rarick KR, et al. Astrocytes directly influence tumor cell invasion and metastasis in vivo. *PLoS One*. 2013;8:e80933.
49. Hajal C, Le Roi B, Kamm RD, Maoz BM. Biology and models of the blood–brain barrier. *Annu Rev Biomed Eng*. 2021;23:359-384.
50. Bos PD, Zhang XH-F, Nadal C, et al. Genes that mediate breast cancer metastasis to the brain. *Nature*. 2009;459:1005-1009.
51. Epshtein Y, Blau R, Pisarevsky E, et al. Polyglutamate-based nanoconjugates for image-guided surgery and post-operative melanoma metastases prevention. *Theranostics*. 2022;12:6339.
52. Ishida Y, Agata Y, Shibahara K, Honjo T. Induced expression of PD-1, a novel member of the immunoglobulin gene superfamily, upon programmed cell death. *EMBO J*. 1992;11:3887-3895.
53. Taggart D, Andreou T, Scott KJ, et al. Anti–PD-1/anti–CTLA-4 efficacy in melanoma brain metastases depends on extracranial disease and augmentation of CD8+ T cell trafficking. *Proc Natl Acad Sci*. 2018;115:E1540-E1549.
54. Lim SY, Yuzhalin AE, Gordon-Weeks AN, Muschel RJ. Targeting the CCL2-CCR2 signaling axis in cancer metastasis. *Oncotarget*. 2016;7:28697.
55. Hao Q, Vadgama JV, Wang P. CCL2/CCR2 signaling in cancer pathogenesis. *Cell Commun Signal*. 2020;18:1-13.
56. Jin J, Lin J, Xu A, et al. CCL2: An important mediator between tumor cells and host cells in tumor microenvironment. *Front Oncol*. 2021;11:722916.
57. Kadomoto S, Izumi K, Mizokami A. Roles of CCL2-CCR2 axis in the tumor microenvironment. *Int J Mol Sci*. 2021;22:8530.
58. Ling Z, Li W, Hu J, et al. Targeting CCL2-CCR4 axis suppress cell migration of head and neck squamous cell carcinoma. *Cell Death Dis*. 2022;13:158.
59. Tsuyada A, Chow A, Wu J, et al. CCL2 mediates cross-talk between cancer cells and stromal fibroblasts that regulates breast cancer stem cells. *Cancer Res*. 2012;72:2768-2779.
60. Valković T, Lučin K, Krstulja M, Dobi-Babić R, Jonjić N. Expression of monocyte chemotactic protein-1 in human invasive ductal breast cancer. *Pathol Res Pract*. 1998;194:335-340.

61. Ueno T, Toi M, Saji H, et al. Significance of macrophage chemoattractant protein-1 in macrophage recruitment, angiogenesis, and survival in human breast cancer. *Clin Cancer Res*. 2000;6:3282-3289.
62. Saji H, Koike M, Yamori T, et al. Significant correlation of monocyte chemoattractant protein-1 expression with neovascularization and progression of breast carcinoma. *Cancer*. 2001;92:1085-1091.
63. Chavey C, Bibeau F, Gourgou-Bourgade S, et al. Oestrogen receptor negative breast cancers exhibit high cytokine content. *Breast Cancer Res*. 2007;9:1-11.
64. Nam J-S, Kang M-J, Suchar AM, et al. Chemokine (CC motif) ligand 2 mediates the prometastatic effect of dysadherin in human breast cancer cells. *Cancer Res*. 2006;66:7176-7184.
65. Dutta P, Sarkissyan M, Paico K, Wu Y, Vadgama JV. MCP-1 is overexpressed in triple-negative breast cancers and drives cancer invasiveness and metastasis. *Breast Cancer Res Treat*. 2018;170:477-486.
66. Fang WB, Jokar I, Zou A, Lambert D, Dendukuri P, Cheng N. CCL2/CCR2 chemokine signaling coordinates survival and motility of breast cancer cells through Smad3 protein-and p42/44 mitogen-activated protein kinase (MAPK)-dependent mechanisms. *J Biol Chem*. 2012;287:36593-36608.
67. Fang WB, Sofia Acevedo D, Smart C, et al. Expression of CCL2/CCR2 signaling proteins in breast carcinoma cells is associated with invasive progression. *Sci Rep*. 2021;11:8708.
68. Fang WB, Yao M, Jokar I, et al. The CCL2 chemokine is a negative regulator of autophagy and necrosis in luminal B breast cancer cells. *Breast Cancer Res Treat*. 2015;150:309-320.
69. Kanyomse Q, Le X, Tang J, et al. KLF15 suppresses tumor growth and metastasis in triple-negative breast cancer by downregulating CCL2 and CCL7. *Sci Rep*. 2022;12:19026.
70. O'Hayre M, Salanga CL, Handel TM, Allen SJ. Chemokines and cancer: Migration, intracellular signalling and intercellular communication in the microenvironment. *Biochem J*. 2008;409:635-649.
71. Li J-Y, Ou Z-L, Yu S-J, et al. The chemokine receptor CCR4 promotes tumor growth and lung metastasis in breast cancer. *Breast Cancer Res Treat*. 2012;131:837-848.
72. Fujimoto H, Sangai T, Ishii G, et al. Stromal MCP-1 in mammary tumors induces tumor-associated macrophage infiltration and contributes to tumor progression. *Int J Cancer*. 2009;125:1276-1284.
73. Bozic I, Reiter JG, Allen B, et al. Evolutionary dynamics of cancer in response to targeted combination therapy. *elife*. 2013;2:e00747.
74. Bonapace L, Coissieux M-M, Wyckoff J, et al. Cessation of CCL2 inhibition accelerates breast cancer metastasis by promoting angiogenesis. *Nature*. 2014;515:130-133.
75. Gatti-Mays ME, Balko JM, Gameiro SR, et al. If we build it they will come: Targeting the immune response to breast cancer. *NPJ breast cancer*. 2019;5:37.
76. Page DB, Beal K, Linch SN, et al. Brain radiotherapy, tremelimumab-mediated CTLA-4-directed blockade+/– trastuzumab in patients with breast cancer brain metastases. *NPJ Breast Cancer*. 2022;8:50.
77. Schlam I, Gatti-Mays ME. Immune checkpoint inhibitors in the treatment of breast cancer brain metastases. *Oncologist*. 2022;27:538-547.
78. Han JJ. *FDA Modernization Act 2.0 allows for alternatives to animal testing*. Wiley Online Library; 2023.
79. Datta P, Dey M, Ataie Z, Unutmaz D, Ozbolat IT. 3D bioprinting for reconstituting the cancer microenvironment. *NPJ Precis Oncol*. 2020;4:18.
80. Hickman JA, Graeser R, de Hoogt R, et al. Three-dimensional models of cancer for pharmacology and cancer cell biology: Capturing tumor complexity in vitro/ex vivo. *Biotechnol J*. 2014;9:1115-1128.
81. Zhou Y. Understanding the cancer/tumor biology from 2D to 3D. *J Thorac Dis*. 2016;8:E1484.
82. Workman P, Aboagye E, Balkwill F, et al. Guidelines for the welfare and use of animals in cancer research. *Br J Cancer*. 2010;102:1555-1577.
83. Mak IW, Evaniew N, Ghert M. Lost in translation: Animal models and clinical trials in cancer treatment. *Am J Transl Res*. 2014;6:114.